Morphodynamic Response of Tidal Mudflats to Marine Cohesive Sediment Influx

Wongsoredjo Samor

Master of Science in Earth Sciences Thesis

Utrecht, 2016

Utrecht University, Faculty of Geosciences

Morphodynamic Response of Tidal Mudflats to Marine Cohesive Sediment Influx

Wongsoredjo Samor

Student number: 4226518

Supervisors:

Prof.dr. M.G. Kleinhans

L. Braat, MSc

Utrecht University

Faculty of Geosciences

Department of Physical Geography

Final version, 4 July 2016

Preface

This thesis is written as partial fulfillment in obtaining the Master of Science MSc degree at the Utrecht University, the Faculty of Geosciences, Department of Physical Geography. This thesis focuses on the topic of the effect of mud on estuary morphology.

The topic of estuary morphology was provided by prof. dr. Maarten Kleinhans, and Lisanne Braat MSc. Within the topic of estuary morphology I focused on numerical experiments with tidal mudflat morphology which form part of estuary morphology. The results and findings of this numerical experiments are documented in this thesis report.

Acknowledgements

I would like to acknowledge and express my sincere gratitude to my supervisors Prof. dr. Maarten Kleinhans, and Lisanne Braat MSc. Their valuable insights and directions provided me with the needful guidance to successfully complete this research and to write this thesis. Furthermore I would like to thank dr. Maarten van der Vegt for his valuable insight on modeling tidal induced currents. Lastly, I also want to thank my family and friends who have supported me with tips, advice and comments during my research.

Samor Wongsoredjo, 4 July 2016, Utrecht

Table of Contents

List of Figures and Tables

Abstract

Estuaries adjust their plan form, low water cross-section and intertidal profile to achieve a stable configuration when external changes in sediment fluxes and sediment types occur (Townend, 2010). Tidal mudflats are part of the intertidal profile; tidal mudflats accrete when suspended cohesive sediment influx increases and retreats when sediment influx diminishes (Pritchard & Hogg, 2003). Therefore, morphological changes to tidal mudflat induces changes in the estuary morphology. The stable estuary morphology depends on morphodynamic equilibrium conditions and the relevant processes that induce morphological changes.

Recent studies had still used a pre-determined tidal flat geometry in order to determine stable estuarine morphodynamic equilibrium conditions (Mariotti & Fagherazzi, 2013; Lanzoni & D'Alpaos, 2014). Nonetheless, these studies have shown which relevant processes are needed to form tidal flat and channel morphodynamics. The aim of this study is to illustrate morphological effects of tidal mudflat on the overall estuary morphology by including sand-mud interactions.

This study focuses on tidal mudflat morphology within a funnel shape estuary. A process-based numerical approach is used to simulate tidal mudflat morphodynamics with the following processes: 1) tide-generated currents, 2) wave generated currents, 3) fluvial discharge, 4) fluvial non-cohesive sediment influx, and 5) marine cohesive sediment influx. Waves were not simulated properly in the model configuration used in this study.

Model results suggest that tidal mudflats are wider in the estuary mouth and become narrower further upstream. The tidal mudflat widths upstream can become wider when the mud suspended load increases upstream. Lateral migrating channel bends can induce a local narrowing of tidal mudflat by erosion. Furthermore the length scales of estuary width are lower when cohesive sediment influx is included and higher when cohesive sediment influx is absent. Length scale of estuary depth decreases for simulations with cohesive sediment influx while the length scale of depth increases for the simulations without cohesive sediment influx.

1 Introduction

Estuaries are important for transport of material, recreation and other economic activities. For such reasons it is important to keep the estuary functioning for humans and its natural habitat. Any change in estuary morphology by anthropogenic causes may result in detrimental long-term changes. Such morphological changes can at present be simulated better by improved sediment transport equations (Dam and Bliek, 2011). However, the morphodynamic conditions for long-term morphological changes still requires further research (Mariotti & Fagherazzi, 2013).

Conditions to determine channel-tidal flat morphodynamic equilibrium, for example, still require an assumed tidal flat geometry to determine the stable equilibrium conditions although knowledge on tidal mudflats has advanced throughout the past years (Mariotti & Fagherazzi, 2013; Lanzoni & D'Alpaos 2014). Having knowledge of morphodynamic equilibrium conditions can determine the length of morphological response times and pathways towards when determining which natural morphological changes takes place (Cowell & Thom, 1997).

Tidal mudflats are one of the gross properties of estuary morphology along with estuary planform and low water channel cross sectional shape (Townend, 2010, 2012). Tidal mudflat morphology can be coupled through hydraulic equations (Townend, 2010, 2012) or to both hydraulic and explicit sediment transport formulations (Mariotti & Fagherazzi, 2013). Attaining uniform velocity along a cross-shore profile of tidal mudflat is a condition for tidal mudflat to reach morphodynamic equilibrium when taking into account only hydraulics (Friedrichs, 2011).

Mariotti & Fagherazzi (2013) have used equal sediment concentration in all morphological elements as a condition to model tidal mudflat equilibrium morphology. Both the simulations by Townend (2010, 2012) and Mariotti & Fagherazzi (2013) have assumed an equal suspended sediment concentration in the channel of their morphodynamic simulations in order to let their simulations reach morphodynamic equilibrium.

However, for an estuary which includes processes on different time and spatial scales morphodynamic equilibrium has been defined as a state in which dissipation energy of morphodynamic processes are minimized (Van der Wegen et al., 2008). In the estuarine morphodynamic simulations of Van der Wegen et al.(2008) only non-cohesive sediment was used. Numerical morphodynamic simulations and experiments for fluvial channels and deltas have suggested different morphological outcomes due to inclusion of different grain sizes or properties (Savenije, 2012; Van Dijk et al., 2013; Caldwell & Edmonds, 2014). An example of different morphological outcomes for deltas are elongated delta planform versus circular delta planform (Caldwell & Edmons, 2014); another example is meandering channel versus braiding channels (Van Dijk et al., 2013).

The aim of this research is to illustrate morphodynamic implications of tidal mudflats to overall estuary morphology by simulations with marine cohesive sediment in numerical simulations. Numerical simulations with tidal and wave induced currents to drive sediment transport in an estuary were used. Furthermore, energy dissipation formulation by Van der Wegen et al. (2008) was used to determine whether morphodynamic equilibrium was reached for simulations with cohesive sediment.

Morphological changes to tidal flats and channels to cohesive sediment influx, tides and waves are presented in current thesis report. In this introductory chapter the problem description, research questions, and hypothesis have been presented. Chapter two will review issues presented from previous research. The preceeding chapter will describe the methodology used in current research. In chapter four the results of current research is presented. The thesis concludes with a chapter on the discussion and conclusions.

2 Review of Tidal Mudflats Morphodynamic in Estuaries

2.1 Introduction

Estuaries adjust their planform, low water channel and intertidal areas to a stable morphological state when external sediment and water fluxes change (Townend, 2010, 2012). Several studies have illustrated stable estuary morphologies under different system parameters, as well as initial and boundary conditions (Van der Wegen et al., 2008; Lanzoni & D'Alpaos, 2014). Initial conditions maybe different factors such as morphological schematization (Mariotti & Fagherazzi, 2013) or sediment grain size distribution (Van Dijk et al., 2013; Caldwell & Edmonds, 2014).

Higher percentages of clay in a sediment matrix have been used to illustrate the increase of erosion resistance of a channel bed or channel bank (Van Ledden, 2003; Grabowski et al., 2011; Van Dijk et al., 2013; Caldwell & Edmonds, 2014). Hence, tidal flats composed of clay in an estuary will be more resistant to erosion by tide or wave generated currents.

Tidal flat morphodynamics can be affected by different factors such as: external sediment influx, tidal range, tidal asymmetry, waves, and sediment characteristics (Friedrichs, 2011; Mariotti & Fagherazzi, 2013).

Morphodynamic response of tidal flats in turn can affect channel morphology (Mariotti & Fagherazzi , 2013; Tambroni & Seminara, 2012). A convex-up tidal flat profile results in a narrower channel width, while a concave-up cross-shore profile results in a wider channel width (Bearman et al., 2010; Townend, 2012). Another feature of tidal flats is the ability of storing or delivering suspended sediment to an adjacent channel. Tidal flats are mostly sinks of suspended sediments under tide generated currents, while tidal flats are mainly sources of suspended sediment under dominating wave generated currents.

An interaction between channel and tidal flat morphology has been illustrated by several studies. Some effects of this interaction are: a deeper or shallow channel (Mariotti & Fagherazzi, 2013), and a shorter tidal channel (Seminara et al., 2010). Tidal flat – channel interaction may not result in a static morphology, but in a dynamic changing morphology while still maintaining a stable channel geometry; outer river banks erode when a meandering channel migrates towards the outer bank, while sediment is deposited on the inner channel bend. This has been noticed to take place under cohesive and non-cohesive sediment mixture (Van Dijk et al., 2013).

Morphological changes between a tidal flat and a channel flat can become negligible on a long temporal scale; such state with negligible morphological changes is said to be in morphodynamic equilibrium (Wright & Thom, 1997; Mariotti & Fagherazzi, 2013). Different conditions are reported in previous studies to determine whether a tidal flat-channel morphodynamic system has approached equilibrium. Two conditions for morphodynamic equilibrium are: uniform suspended sediment concentration (Mariotti & Fagherazzi, 2013), and minimum energy dissipation (Van der Wegen et al., 2008). These morphodynamic equilibrium do not explicitly take into account the effect of combined cohesive and non-cohesive sediment.

A continuum of tidal flat – channel morphology will be reviewed in this chapter. Mainly the tidal flat-channel morphology composed of cohesive sediment will be further elaborated on with an emphasis morphodynamic equilibrium.

First, some previous studies on mechanisms of tidal flat morphodynamics in the setting of an estuary morphology are presented; then followed by investigations done on channel morphodynamics interacting with tidal flats. The different morphological outcomes from such studies will be compared in this review. This comparison will be followed by a synthesis, problem description, research questions, and hypothesis for further studies.

2.2 Morphodynamics of Tidal Mudflats

Tidal flat morphodynamics is affected by processes such as: sediment influx, tidal range, tidal asymmetry, and waves (Friedrichs & Aubrey, 1995; Roberts et al. 2000; Pritchard et al. 2002; Pritchard & Hoggs, 2003; Bearman et al., 2010; Friedrichs, 2011). These processes are summarized in Figure 1. Tidal flat morphology will change by these processes until morphodynamic equilibrium is reached.

Tidal flats in morphodynamic equilibrium under tidal currents have a convex-up profile, while tidal flats in morphodynamic equilibrium under wave generated currents have a concave-up tidal flat profile (Friedrichs, 2011). Tidal flat are in dynamic equilibrium when forced by both tide and wave generated currents (Friedrichs, 2011; Hu et al., 2015). Erosion and deposition are balanced on tidal profiles under morphodynamic equilibrium. However, when deposition exceeds erosion tidal flat progradation takes place (Maan et al., 2015). Increased deposition is a result of morphodynamic interaction between upper and lower tidal flat (Maan et al., 2015). The following paragraphs will elaborate further on above mentioned tidal flat morphodynamic processes.
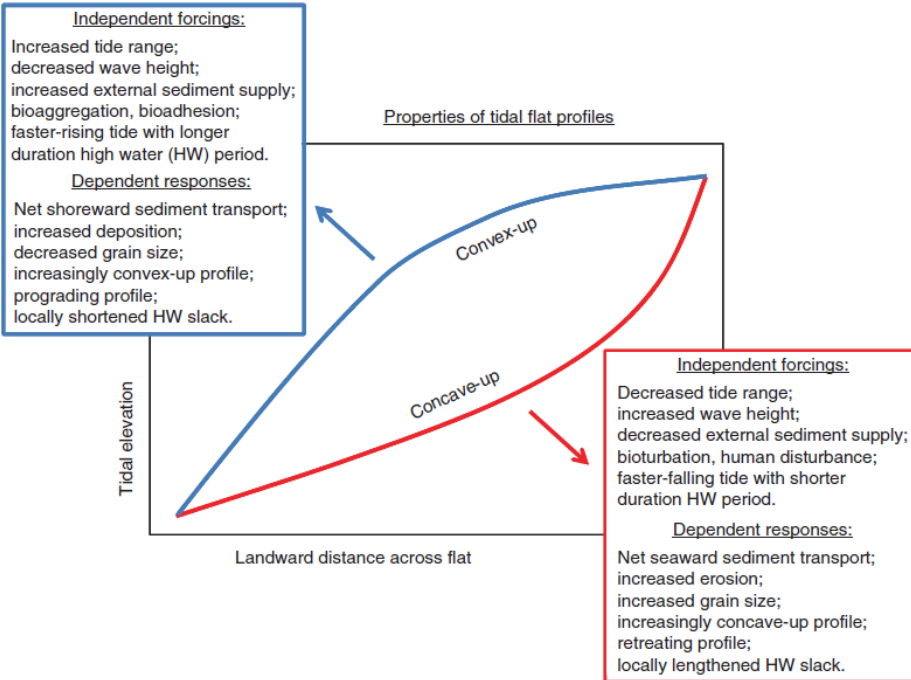
Figure 1: Theoretical tidal mudflat equilibrium morphology depending on the dominant hydrodynamic forcings. Hydrodynamic forcings in this case are tidal range, wave height, sediment supply, and asymmetry in tidal currents and slack durations(source: Friedrichs, 2011)

Tide generated currents and bed shear stress over a linear sloping tidal flat (Figure 2) have non-uniform spatial distribution (Figure 3a). This non-uniformity cause a gradient along the tidal flat and drive a net sediment transport towards the landward end of the tidal flat (Friedrichs & Aubrey, 1996).
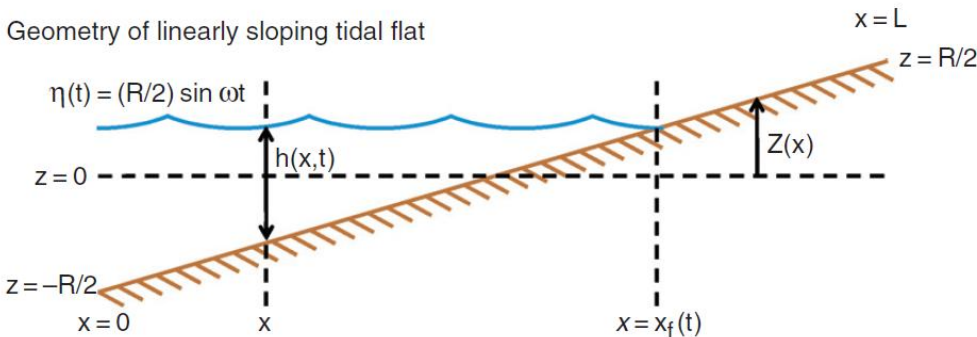
Figure 2: Initial bed level for analysis of tidal flat equilibrium morphology. Elements for analyzing tidal flat equilibrium morphology are: mean water level (z=0), low water level (z= -R/2), high water level (z=R/2), lower end of tidal flat (x=0), higher end of tidal flat (x= L), water level (h), bed level with respect to mean water level (Z), and water level fluctuations by tides (η). X indicate position along the tidal flat, X_f indicates the tidal front (Source: Friedrichs, 2011).
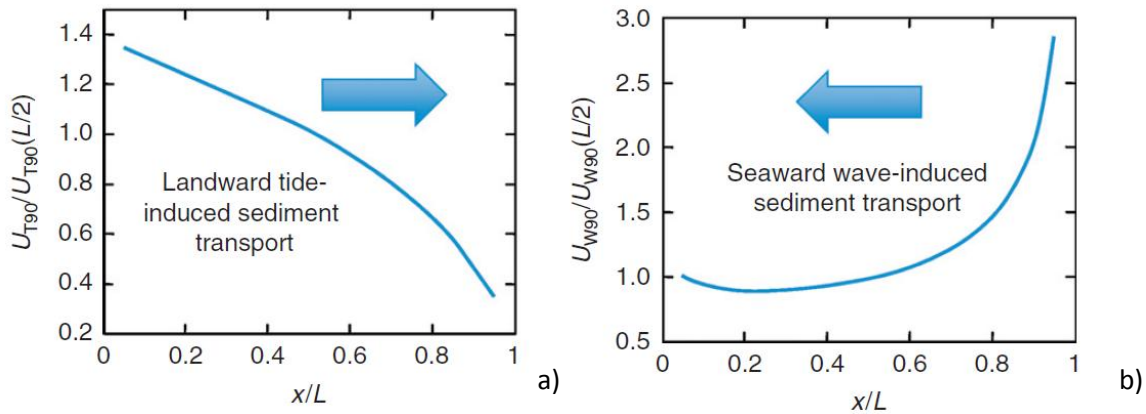
Figure 3: Spatial gradients in energy caused by tide induced currents and wave induced currents along non-dimensional distance along a tidal flat. The left graph (panel a)represent tide induced currents, while the right graph (panel b) represents wave induced currents. Sediment transport is from the high to low energy (Source: Friedrichs, 2011).

Waves acting on tidal flats cause a net current and bed shear stress gradient in seaward direction (Figure 3b). Sediment is transported towards the seaward end (Friedrichs & Aubrey, 1995; Friedrichs, 2011).

In order to have morphodynamic equilibrium on a tidal flat, a zero gradient in bed shear stress is needed along the cross-shore profile of the tidal flat. This condition of zero gradient in bed shear stress goes for both the tide and wave generated currents (Friedrichs & Aubrey, 1995; Friedrichs, 2011). A way to achieve zero gradient bed shear stress is to adjust the tidal flat cross shore profile. The profile will change from linear to a static convex-up for the tide dominated case, and static concave-up for the wave dominated case (Friedrichs & Aubrey, 1995; Friedrichs, 2011).

Tidal flat slopes can become steeper when tidal ranges increases under conditions of maximum uniform bed shear stress (Roberts et al., 2000; Friedrichs, 2011). Maximum bed shear stresses remain the same for tides when tidal periods remain the same; although tidal ranges are varied. For tidal flats with increased tidal ranges to remain in morphodynamic equilibrium the bed slope needs to become steeper (Friedrichs, 2011).

By increasing the sediment supply at the offshore boundary of a tidal flat, the amount of deposition increases. Hence, the cross shore width becomes wider under tidal conditions (Roberts et al., 2000). Deposition will continue until erosion will balance the deposition. When erosion balances the deposition there will be no net bed level change, hence the tidal flat has achieved morphodynamic equilibrium (Roberts et al., 2000).

Asymmetric tides can also cause tidal flats to be convex-up, followed by tidal flats progradation or retreat (Pritchard et al., 2002; Pritchard & Hogg, 2003). Morphodynamic equilibrium for asymmetric tidal conditions still hold; i.e. maximum tidal currents need to be uniform over tidal flat. Therefore the cross shore profile is always convex up. However, when asymmetric tides are flood dominated and a sediment supply persists, a net landward sediment transport prevails. Uniform maximum tidal currents must still be present to have morphodynamic equilibrium, hence the tidal flat remains convex-up while prograding (Pritchard et al., 2002). Tidal flat retreat occurs when tides are asymmetric and ebb-dominant. Net sediment transport is directed offshore which results in sediment being removed from the tidal flat (Pritchard et al., 2002). Asymmetric tides can also refer to a longer slack water during high tide compared to duration of slack water during low tide (Friedrichs, 2011). It is expected that more sediment can deposit during a longer slack water period (Friedrichs, 2011).

Interaction within a tidal flat morphology affects the direction of sediment transport resulting in a prograding or retreating tidal flat (Maan et al., 2015). The phenomenon of *tidal flat profiles progradation* in morphological studies indicate that a tidal flat profile is advancing in seaward direction due to enhanced sedimentation (Pritchard et al., 2002). A condition for a tidal flat to prograde is the presence of sediment supply from the offshore boundary.

Tidal currents on tidal flats drive a feedback between lower tidal flat and upper tidal flat (Figure 4). This feedback between lower tidal flat and upper tidal flat is a result between tidal currents and bed slope (Maan et al., 2015). The following formula is a basis of the feedback between lower tidal flat and upper tidal flat (Friedrichs & Aubrey (1996); Le Hir et al. (2000) in Maan et al. (2015):

$$u(x) = \frac{\pi R}{\beta T_{tide}} \qquad\qquad eq.\,1$$

u(x) is the cross-shore flow velocity along a tidal flat profile

R is the tidal range

β is the average bed slope

T_{tide} is the tidal period

According to equation 1 a low bed slope results in higher cross-shore currents, while a high bed slope results in lower cross-shore velocities. The bed slope of the tidal flat increases when the bed level of upper tidal flat also increases. These processes are summarized in Figure 4. The bed shear stress is a result of cross-shore flow velocities. In short, mainly the bed slope between the upper and lower tidal flat is important to balance cross-shore flow velocities and sedimentation on the lower flat and on the upper flat (Maan et al., 2015).

For wave and tide case (see Figure 5) tidal mudflat progradation is possible when net sedimentation takes place on both the Lower and Upper flat. Summarized, a wave and tide case affects the feedback between Upper flat and Lower flat. Of great importance in this feedback is the wave-induced bed shear stress which is depth limited. This means that waves exert higher bed shear stress in relatively shallow water depth and lower bed shear stress in relatively deep water depth. Therefore, the Upper flat is eroded while the deposition takes place on the Lower flat. However, the water depth becomes shallow when the Lower flat bed level increases due to sediment deposition.

A shallow water depth over the Lower flat causes wave energy dissipation over the Lower flat, therefore increasing wave induced bed shear stress over the Lower flat. This shift of high bed shear stress region from Upper flat to Lower results in deposition on the Upper flat. If a net deposition takes place on Lower and Upper flat, a net tidal flat progradation is still possible under wave and tide condition (Maan et al., 2015).

Maan et al. (2015) have only considered cross-shore currents in their analysis of tidal mudflat progradation or retreat. However, the response of a tidal mudflat, progradation or retreat, can also explain closure of a channel in a channel bifurcation system (Wang et al., 2015).
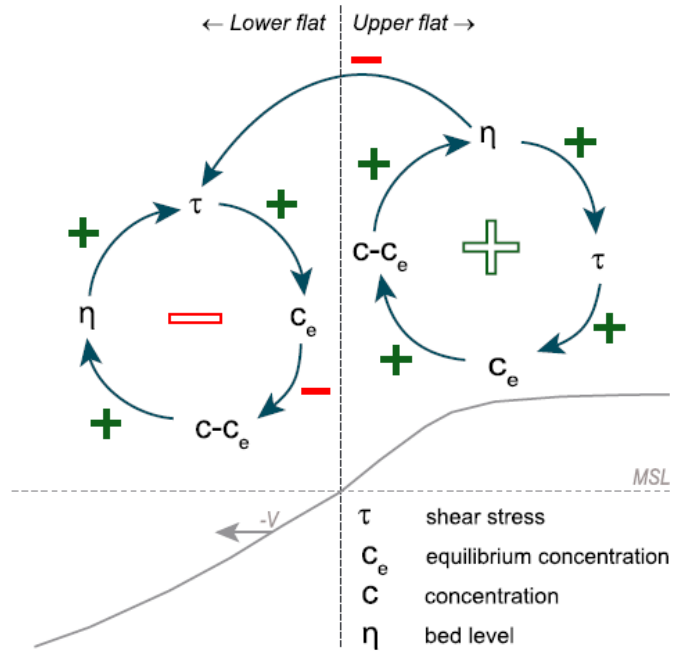
Figure 4: Interaction between upper tidal flat and lower tidal flat driven by tide induced bed shear stress. A low bed slope on either upper and lower tidal flat increases the bed shear stress. Eroded sediment is advected by tidal currents to either part of the tidal flat. Sedimentation takes place where the concentration of advected sediment exceeds the reference concentration (source: Maan et al., 2015).
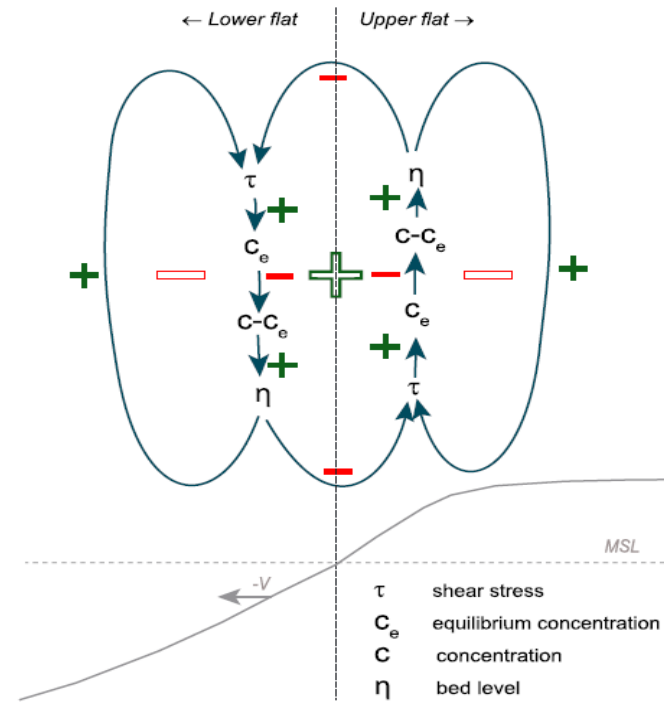
Figure 5: Interaction between upper and lower tidal flat driven by tide- and wave-induced bed shear stresses. Similar to figure 4, sedimentation takes place where concentration of advected sediment exceeds reference sediment concentration. However, the area of high wave induced bed shear stresses shift towards areas which have a significant bed level elevation (source: Maan et al., 2015).

2.3 Interaction between a Channel and Tidal Flats

Channel morphodynamics in estuaries can be forced by hydrodynamic processes and by tidal flat morphodynamics (Mariotti & Fagherazzi, 2013; Van der Wegen et al., 2014). Some known ways how tidal flat interact with channel morphodynamics are: changes in suspended sediment exchange between a tidal flat and a channel (Mariotti & Fagherazzi, 2013), and narrow the width of a channel by shoal margin accretion (Van der Wegen et al., 2014). Channel morphology itself can shift due to shoals formation (Van der Wegen et al., 2008). Such shift in channel morphology may be analog to meandering channels in which a single channel is formed with upstream channel flow going mainly in one direction (Van Dijk et al., 2013). Tidal currents can affect exchange of sediment between tidal flats and a channel by the following factors: 1) spatial difference in bed shear stress by estuary degree of funneling, 2) asymmetry of tidal signals, and 3) trapping of sediment by intersecting tidal currents and fluvial discharge (Friedrichs et al., 1998; Friedrichs, 2011; Pittaluga et al., 2015). These processes will be further elaborated on in the following paragraphs.

Estuary plan form in practice is mostly funnel shape, but the degree of funnel shape convergence varies; a nearly rectangular estuary has a convergence degree of 0, while a funnel shape estuary converges with a degree greater than 0 (Friedrichs, 2010 in Valle-Levinson, 2010; Pittaluga et al., 2015). A greater convergence degree of estuary plan form results in an increase of tidal currents towards the head of an estuary followed by a decrease in magnitude of tidal currents (Friedrichs, 2010 in Valle-Levinson, 2010). However, when channel depth becomes shallower the magnitude of tidal currents decreases (Friedrichs, 2010 in Valle-Levinson, 2010). This competing effect of plan form funneling degree and channel depth can result in a spatial difference in magnitude of tidal currents. Bed shear stresses scale with magnitudes of currents, therefore spatial differences in magnitude of currents also result in spatial differences in bed shear stresses. At location within an estuary with relatively high bed shear stress result in higher suspended sediment concentration. Currents transport this suspended sediment towards areas with low bed shear stress, therefore deposition of sediment takes place (Friedrichs, 2011).

Asymmetry of tidal signals can indicate differences in duration of maximum ebb and flood currents or duration of ebb and flood slack tides. A longer duration in maximum currents result in greater amount of sediment being entrained in suspension (Friedrichs, 2011). Longer slack tide indicates a longer time for sediment to settle to a channel or tidal flat bed, hence more deposition of sediment takes place (Friedrichs, 2011).

An upstream river discharge can also be present at an estuary head resulting in an intersection between a seaward directed river flow and upstream directed flood tidal currents (Friedrichs et al., 1998; Pittaluga et al., 2015). At this intersection suspended sediment concentration increases by "trapping" of suspended sediment (Friedrichs et al., 1998). Increased suspended sediment concentration can results in an increase of tidal flat width at this intersection (Friedrichs & Aubrey, 1995; Roberts et al., 2000; Pritchard & Hogg, 2003; Friedrichs, 2011; Maan et al., 2015).

Morphodynamic equilibrium of tidal flat – channel morphology depend on: volume of water and sediment exchanged between tidal flat and channel, suspended sediment concentration, presence and magnitude of surface water waves, and sea level (Mariotti & Fagherazzi, 2013). A greater volume of water laden with suspended sediment towards tidal flats results in a greater sedimentation. However, water surface waves on tidal flats entrain sediment during high water. Therefore more suspended sediment is transport of towards the channel resulting in a decrease of tidal flat elevation (Mariotti & Fagherazzi, 2013).
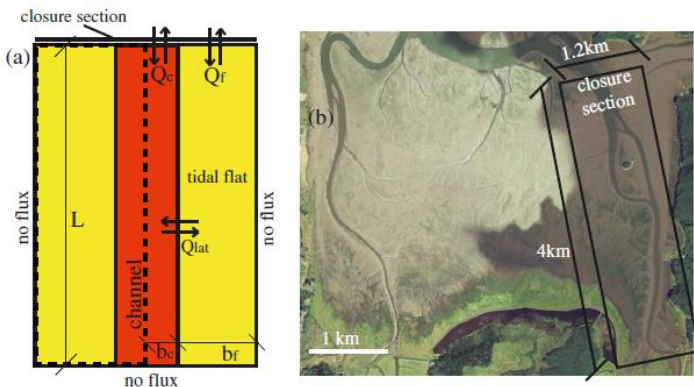
Figure 6: Schematisation of sediment and water exchange between tidal flat and channel (Source: Mariotti & Fagherazzi, 2013). Qc is discharge of sediment and water in the channel, Qf is discharge of sediment and water over a tidal flat, Qlat is discharge of sediment and water between channel and tidal flat. bc is channel width, bf is flat width in the model by Mariotti & Fagherazzi (2013). No flux indicates closed boundaries, closure section indicates inlet boundary of the numerical model by Mariotti & Fagherazzi (2013).

Depending on initial flat and channel depth, and the presence of waves a continuum of stable tidal flat-channel morphodynamic equilibria can be possible (Mariotti & Fagherazzi, 2013). Mariotti & Fagherazzi (2013) showed that tides result in a tidal flat elevation near high water and a channel depth lower than low water. With waves the tidal flat elevation is reduced to elevations near low water level or lower. These stable morphodynamic equilibrium have been attained under the following conditions: 1) spatially uniform suspended sediment

concentration along the channel and tidal flat, 2) tidal flat and channel bed elevation changes in vertical direction, and 3) uniform water level, and currents along the tidal flat and channel.

A channel changes it's width when an adjacent shoal width changes; i.e. a wider shoal results in a narrow channel while a narrow shoal results in a wider channel (Van der Wegen et al., 2014). Sediment for shoal margin accretion can be supplied from a river, shoal or tidal flat (Van der Wegen et al., 2014). A river supplies sediment due to increased upstream sediment influx. Sediment is entrained from tidal flat and shoal bed by wave-induced bed shear stresses and transported by ebb tidal currents towards the shoal margin. However, when upstream sediment flux and waves are absent the channel width increases (Van der Wegen et al., 2014).

Shoals in a channel can affect current directions which result in morphological changes of a channel (Hibma et al., 2003; Van der Wegen et al., 2014). A morphological change can be channel bank erosion which is caused by currents directed toward a channel bank (Van der Wegen et al., 2008). Currents directed toward a channel bank can shear along the outer bend of a channel before flowing back into a straight part of a channel (Constantinescu et al., 2013). Sediment is entrained from the outer bend by currents shearing along the channel bank, therefore resulting in outer bend channel bank erosion.

Estuary morphodynamics can also be affected by lateral channel migration (Van Dijk et al., 2013). Lateral channel migration of tidal meanders take place by erosion of outer bend channel banks which is balanced by deposition of sediment on inner bend of a channel bank (Van Dijk et al., 2012). Tidal flats along channel estuary channel banks are likely to get affected by lateral channel migration; a spatial difference in tidal flat width may result. Other morphological changes due to lateral channel migration are channel bed erosion and channel bank failure due to the undermining by currents (Kleinhans et al., 2009).

Morphological behavior of either channel bed or channel bank depend on sediment characteristics (Van Dijk et al., 2013; Caldwell & Edmonds, 2014). The ratio of mud and sand is one way of characterizing sediment erosion resistance; sediment becomes more resistant to erosion when clay content increases (See Figure 7) (Torfs, 1995 in van Ledden, 2003). River floodplains for example are able to form at the inner bends of a meander when cohesive sediment is supplied by the river (Van Dijk et al., 2013). These floodplains are therefore able to constrain upstream discharge and river dynamics within a single channel; therefore forming a meandering channel (Van Dijk et al., 2013).
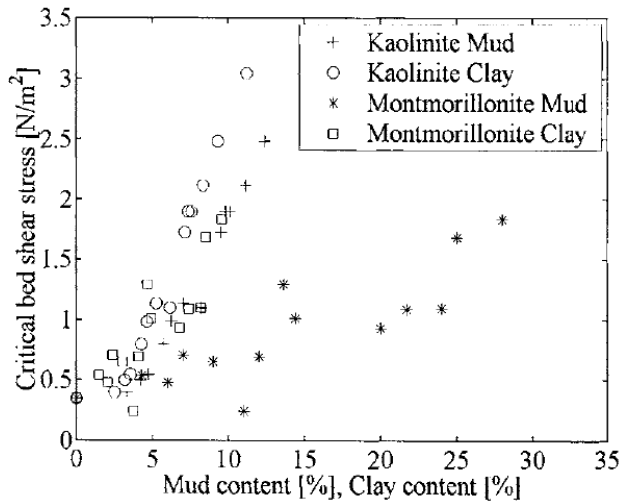
Figure 7: Critical bed shear stresses as function of mud and clay content. The Kaolonite Mud contains 4% mud, Montmorillonite Mud has 13% mud, Kaolonite clay contains 3% clay, and Montmorillonite clay consists of 4% clay. Comparing Montmorillonite Mud and Montmorillonite Clay it is shown that clay content is mainly important in determining Critical bed shear stress (source: Torfs, 1995 in Van Ledden, 2002)

2.4 Morphodynamic Equilibrium of a Combined Channel and Tidal Flat System

A morphodynamic system composed of a channel and tidal flats can posses a continuum of morphodynamic equilibrium by changing external processes such as: tidal currents, waves and suspended cohesive sediment transport (Mariotti & Fagherazzi, 2013). A balance needs to present between external processes along with channel and tidal flat morphology to achieve equilibrium (Cowell & Thom, 1997). Van Dijk et al. (2013) and Caldwell & Edmonds (2014) illustrated the significant effect of cohesive sediment influx to an estuary. The findings by Van Dijk et al. (2013) and Caldwell & Edmonds (2014) showed that by adding cohesive sediment to a morphodynamic system the erosion resistance of channel banks increased; different estuary morphological configurations can be formed. Caldwell & Edmonds (2014) assumed morphodynamic equilibrium to be achieved when no net changes are observed in channel morphology. Other possible conditions for morphodynamic equilibrium can be zero net spatial gradients in hydrodynamic forces and sediment supply (Mariotti & Fagherazzi, 2013; Van Dijk et al., 2013; Caldwell & Edmonds, 2014; Maan et al., 2015). These conditions will be reviewed and conclude on the applicability to combined channel and tidal flat morphodynamic systems composed of both sand and cohesive sediments.

Spatially uniform suspended sediment concentration is a way of specifying morphodynamic equilibrium beforehand (Mariotti & Fagherazzi, 2013). This condition, zero gradient in sediment concentration leading to negligible morphological changes, is similar to the condition of tidal flat equilibrium imposed by Friedrichs & Aubrey (1995); i.e. zero gradients in bed shear stress

along cross-shore profile of a tidal flat. Applicability of such equilibrium conditions are limited to: 1) combined channel and tidal flat morphodynamic model in which channel width changes are negligible, and 2) composed of a single representative grain size.

Net zero morphological changes is another condition to determine whether a morphodynamic system is in equilibrium or not (Friedrichs, 2011; Hu et al., 2015). This condition explicitly takes into account the periodic hydrodynamic forces which can change morphology. A tidal flat for example will be eroded by waves, but that same volume of sediment lost will be regained by tidal currents (Roberts et al., 2000; Friedrichs, 2011; Hu et al., 2015). Such hydrodynamic forces are assumed to be constant during the length of time being studied. Therefore, tidal flats or other morphological features that maintain a net zero morphological change are referred to as dynamic equilibrium (Friedrichs, 2011; Hu et al., 2015).

Minimum energy dissipation is a different condition to determine whether a channel is in morphodynamic equilibrium (Rodriguez et al., 1992; Van der Wegen et al., 2008). Mainly three principles must be followed to predict a channel cross-section and channel structure which can efficiently convey water and sediment while still maintaining a stable morphology (Rodriguez et al., 1992; Van der Wegen et al., 2008). These principles are: *"(1) the principle of minimum energy dissipation in any link of the network (a local optimal condition), (2) the principle of equal energy dissipation per unit area of channel anywhere in the river network (a local optimal condition normalized by the topographical characteristics of the local area), and (3) the principle of minimum energy dissipation in the network as a whole".* (Rodriguez et al., 1992; Van der Wegen et al., 2008)*.* These principles have been used to illustrate a correspondence in morphodynamic evolution and energy dissipation in channel networks (Rodriguez et al., 1992), and alluvial estuaries (Van der Wegen et al., 2008). Results have shown minimum morphodynamic changes corresponding to minimum energy dissipation (Rodriguez et al., 1992; Van der Wegen et al., 2008). The limitations of using minimum energy dissipation are: 1) only applicable to channels consisting of one sediment grain size, and 2) only tide dominated or fluvial dominated channels.

Morphodynamic equilibrium conditions may not hold for horizontal accreting or retreating tidal flat width (Maan et al., 2015). Cross shore profile can remain in equilibrium, but the horizontal width of a tidal flat changes by accretion or retreat (Maan et al., 2015). However, when tidal flat width increases tidal currents tend to be more ebb-dominant (Dyer et al., 2000). Therefore, sediment in suspension will be transported away from the tidal flat during low tide (Dyer et al., 2000). Clearly the processes considered by Maan et al. (2015) resulted in positive feedback, meaning that there were no other morphodynamic processes to cease accretion or retreat of tidal flats. Ebb-dominated flow may be a processes to have a negative feedback on tidal flat accretion or retreat, therefore horizontal migration of tidal flat could decrease. A

morphodynamic equilibrium will result when positive feedback and negative feedback of morphodynamic processes balance each other (Cowell & Thom, 1997).

2.5 Synthesis

Previous paragraphs have reviewed processes and equilibrium conditions of a combined tidal flat and channel morphodynamic system. A main conclusion from those reviews is that estuary width and depth are affected by changes to tidal flat elevation and width (Mariotti & Fagherazzi, 2013; Van der Wegen et al., 2014).

Several processes that determine tidal flat elevation are: tidal range, tidal currents, waves, sediment characteristics and sediment supply (Friedrichs & Aubrey, 1995; Roberts et al. 2000; Pritchard et al. 2002; Pritchard & Hoggs, 2003; Bearman et al., 2010; Friedrichs, 2011). Tidal flats can be in dynamic morphodynamic equilibrium with a cross shore profile between convex-up and concave-up (Friedrichs, 2011; Hu et al., 2015). A continuous supply of suspended sediment can cause tidal flat width to increase while still maintaining a stable cross-shore profile shape (Maan et al., 2015). An increase in tidal flat width may result in channel width narrowing (Van der Wegen et al., 2014). On the other hand, waves cause tidal flat width to decrease (Friedrichs, 2011).

Tidal flat width can also be determined by the balance between sedimentation and erosion by migrating channels. Migrating channels along a tidal flat can decrease sediment balance by lateral migration (Van Dijk et al., 2013) and channel bank erosion (Kleinhans et al., 2009; Constantinescu et al., 2013). Lateral channel migration is a characteristic of meandering rivers by which channel bank erosion takes place in outer channel bends and floodplain formation in the inner channel (Van Dijk et al., 2013). Channel bank erosion takes place by shearing of currents along the outer channel bank (Constantinescu et al., 2013). Adapting the concept of lateral channel migration to a tidal situation may explain tidal flat width reduction for an estuary dominated by tidal currents only. Not only meandering rivers cause currents to deflect to a channel bank, but also shoals formed on a tidal channel bed (Hibma et al., 2003; Van der Wegen et al., 2008). Shoal formation has been used to illustrate inherent instabilities in channel beds composed of sand (Hibma et al., 2003; Van der Wegen et al., 2008).

Several conditions had been used by previous investigations to predict a channel and tidal flat morphodynamic equilibrium. Two of these conditions are: 1) spatially uniform suspended sediment concentration, and 2) net zero morphological changes. However, these conditions take into account a limited number of processes.

Other processes may prevent tidal flats and channels from reaching morphodynamic equilibrium. Such processes can be: 1) feedback between upper and lower tidal flat (Maan et al., 2015), 2) sand and mud interaction (Van Ledden, 2004; Caldwell & Edmonds, 2014), 3) lateral channel migration (Dijk et al., 2013), and 4) formation of shoal on a channel bed (Hibma et al., 2003; Van der Wegen et al., 2008). Application of these processes to tidal flat and channel morphodynamics within an estuary are scarce while studies had illustrated the importance of these processes on estuary morphology (Van der Wegen et al., 2008, Van Dijk et al., 2013, and Caldwell & Edmonds, 2014). These processes can cause tidal flat width to vary along an estuary.

Previous studies had focused little on simulating tidal flat width variation that included both fluvial sand and marine cohesive sediment influx. Furthermore, tidal flat width had been predefined in simulations of previous studies. Such configurations in simulations may not accurately predict long term morphological evolution to external conditions such as sea level rise. Therefore, studies regarding tidal flat and channel morphodynamics with combined sand and cohesive sediment are needed. This study will focus on tidal flat and channel morphodynamics within an estuary composed of sand and cohesive sediment. The aim of this study is to analyze tidal flat width spatial differences in an estuary morphological composed of mixed non-cohesive and cohesive sediment.

2.6 Research Questions

The following research questions have been posed for this study:

1. What is the morphological response of tidal flats in an estuary due to an increased marine cohesive sediment input compared to only non-cohesive sediment river influx?
2. How much will tidal flat width vary alongshore an estuary with offshore surface water waves compared to tidal currents only?
3. How wide are tidal mudflats for simulations with and without marine cohesive sediment influx?

2.7 Hypothesis

The hypotheses on morphodynamic simulations in this study are:

1. Tidal flat elevation and width will increase to increased sediment influx. The tidal flats will be composed of non-cohesive sediment when either the amount of non-cohesive or cohesive sediment is abundant. The tidal flats close to an estuary mouth will be wider and composed mostly of mud compared to tidal flats further upstream.
2. Tidal currents increase tidal flat width and elevation while waves decrease tidal flat width and elevation. The magnitude of tide and wave generated currents decrease in upstream direction within an estuary. Therefore, tidal flat width and elevation decrease from estuary mouth to estuary head in a tide dominated estuary. Waves generated offshore of an estuary will cause tidal flat width and depth to decrease at an estuary mouth.
3. An estuary mouth provides space for tidal flat width and elevation to increase while further upstream this space decreases. However, marine cohesive sediment influx decreases upstream therefore limiting tidal flat width. The ratio of tidal flat and estuary width remains constant along an estuary. Without marine sediment influx no tidal mudflat will be formed.
4. Shoals on estuary channel bed will deflect current towards channel bends. Currents deflected toward a channel bank increase bed shear stresses at this location. Therefore, erosion of tidal flats at these locations take place.

All four hypotheses will be tested with a process-based numerical model. A comparison of tidal flat width along the modeled estuary will be done by normalizing tidal flat width with total estuary width. Channel bank accretion or retreat at outer bends of the simulation will be graphed with respect to time.

3 Methodology

The main objective of this study was to determine spatial differences in tidal flat width in an estuary with marine cohesive sediment (mud) influx. Delft3D Hydro-Morphodynamic process-based numerical modeling software was used in this study. All simulations started from an 'ideal estuary' which was in morphodynamic equilibrium; i.e. a zero gradient in water level and flow velocity (Savenije, 2012). Changes in morphology due to inherent instability of a sand channel bed were compared to this initial condition. The numerical model was run with various combinations of tides, waves, and cohesive sediment influx. First the model settings in Delft3D modeling software will be given. Then a description on the analysis will be given. The morphological and hydrodynamic model results will be analyzed on: 1) width and depth, 2) tidal prism through and inlet cross sectional area, 3) channel bank displacement by migrating channels, and 4) minimum energy dissipation.

3.1 Model Parameter Settings in Delft3D

Delft3D numerical model includes the following processes: 1) current velocity and direction, 2) transport of non-cohesive and cohesive sediment transport, and 3) bed level update composed of both non-cohesive and cohesive sediment. The reader is referred to Delft 3D-FLOW manual (Deltares, 2014) for details on the formulas programmed in Delft3D. Instead the variables in which have been used to test the hypotheses of this study will be elaborated on. The variables which have been focused on are: 1) suspended cohesive sediment concentration and 2) wave height.

Table 1: Summary of changed parameters in simulations

Processes included	*Sediments*	*Concentration of cohesive sediment influx*
Tides only	Non-cohesive only	N/A
Tides only	Non-cohesive and cohesive	0.05 kg/m3
Tides and waves	Non-cohesive only	N/A
Tides and waves	Non-cohesive and cohesive	0.05 kg/m3

Two simulations have been done with either mud or no mud. The influx of sediment takes place through the estuary inlet to represent marine cohesive sediment influx. Furthermore, two additional simulations have been carried out; one of the simulations without waves and the other with a significant wave height of 4 meters.

The model parameters used in this study are illustrated in Table 2. The values of these parameters have remained constant during each simulations. These values have been adapted from Braat et al. (2016). For this study only marine cohesive sediment influx have been varied. Two parameters important for modeling with cohesive sediment are: 1) Settling velocity, and 2) Critical bed shear stress for erosion. These parameters determine the amount of cohesive sediment deposition, but have not been dealt with due to time constraints of this study.

Table 2: Model parameters

Table of main parameters and values			
	Value	Unit	Comments
Sediment parameters			
Sediment 1			Non-cohesive sediment
Reference density for hindered settling	1600	Kg/m^3	
Specific density	2650	Kg/m^3	
Dry bed density	1600	Kg/m^3	
Median sediment diameter	300	μm	D50
Initial sediment layer thickness at bed	15	m	Uniform
Sediment 2			Cohesive sediment
Reference density for hindered settling	1600	Kg/m^3	
Specific density	2650	Kg/m^3	
Dry bed density	1600	Kg/m^3	

Fresh settling velocity	0.25	mm/s	
Saline settling velocity	0.25	mm/s	
Critical bed shear stress for sedimentation	1000	N/m2	Uniform
Critical bed shear stress for erosion	0.2	N/m2	Uniform
Erosion parameter	0.0001	$Kg/m^{-2}s^{-1}$	Uniform
Initial sediment layer thickness at bed	0.05	m	Uniform
Morphology			
Morphological scale factor	400	No unit	
Spin-up time before morphological changes	14400	Minutes	
Minimum depth for sediment calculation	0.05	m	
Sediment transport parameters			
Van Rijn's reference height factor	1	No unit	
Threshold sediment thickness	0.05	m	
Estimated ripple height factor	2	No unit	
Sediment transport formulas			
Engelund-Hansen (1967)			
Calibration coefficient	1	No unit	
bed roughness height (dummy)	0.05	m	

3.2 Estuary Model Description

Long term morphodynamic modeling of an ideal estuary channel geometry is used. An ideal geometry is one in which there is initially zero gradient in water level and flow velocity in the estuary channel (Savenije, 2012). Previous studies have used this approach to scale morphological features to channel length or width (Schuttelaars & de Swart, 1999; Todeschini et al., 2005; Van der Wegen, 2010). In this study the same approach has been used to simulate the long term morphodynamics of an estuary. The estuary dimensions used in this research were designed by Braat et al. (2016) and will be further used for simulations in current research as initial conditions.

3.2.1 Initial Conditions

The estuary in which simulations had been carried out had the following characteristics before the start of the simulations:

1) Length of estuary and upstream river is approximately 20 km
2) Channel width at the mouth is ± 2.7km
3) The cross section of the channel at time t=0 has a rectangular shape.
4) Planform funnel shape with an e-folding length of width (L_W) of approximately 3.7
5) Initial bed slope of the estuary has an approximate length: depth ratio of 4970 : 1
6) Initial e-folding length scale of depth was 15.4.
7) Initial channel bed is composed of non-cohesive sediment (sand with a D50 of 300 µm) with a thin cohesive sediment layer of 5 cm on top of the non-cohesive sediment layer.
8) Depth of estuary at the mouth is 2 m below mean sea level
9) Depth of seaward part is 15 m below mean sea level
10) The seaward part has a rectangular shape and a dimension of 15 km along the western end and 10 km along the Northern and Southern end. This size was needed to prevent the boundaries from interfering with the currents within the seaward part (personal communication with Van der Vegt, M., 2015)
11) Sea bathymetry had no slope.

3.2.2 Model Computational Grid

The computational grid used is rectilinear with one closed and two open water level seaward boundaries, and a water discharge boundary at the estuary head. A rectilinear grid, either two- or three-dimensional, have coordinate axes which are perpendicular to each other (Stover et al, 2016). This computational grid is subdivided into a seaward part, dry land, and estuary part (Figure 8).
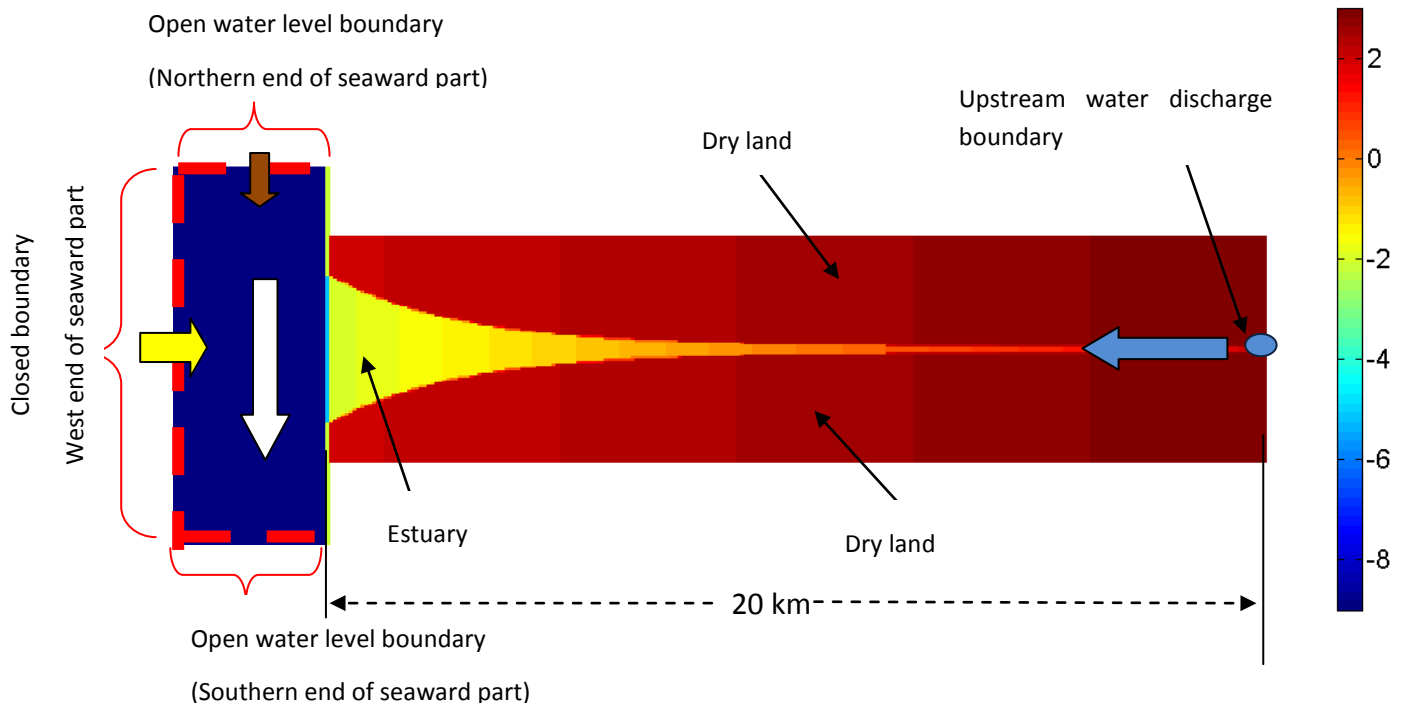
Figure 8: Initial estuary geometry. The white arrow in the seaward part indicates the direction of alongshore tidal wave propagation. The yellow arrow illustrates the direction of wave propagation. The direction of river water discharge and upstream sand flux is shown by the blue arrow. Cohesive sediment influx is illustrated by the brown arrow at the Northern end of the seaward part. The dimensions of the seaward part is 15 km along the western end and 10 km along the Northern and Southern end. The full size of the seaward part is not given in this Figure.

In this figure, the grid cells within the estuary had a mean size of 100 by 100 meters. These grid cells were depicted smaller compared to the grid cells in the ocean part in order to properly simulate flow within the estuary. The magnitude of this decrease was of about the order of two. The computational grid used for current research had dimensions of 15 by 30 km. By placing this computational grid origin at a latitude of 0 decimal degrees (dec.deg) and an orientation of 0 (dec.deg) effects of Coriolis Forces were canceled out.

3.2.3 Boundary Conditions

The external forces which cause morphodynamic changes in the afore mentioned model are: tides, waves, upstream river discharge, and suspended marine cohesive sediment. The boundary conditions to simulate tides, waves and upstream river discharge is given in table 3.

The generation of tidal currents in the seaward part are forced by a harmonic tidal wave. The harmonic tidal wave flow propagates alongshore from the Northern seaward end to the Southern seaward end (Figure 8). A harmonic frequency of 30 deg/h was chosen for the following purposes: 1) approximate an M2 tidal constituent, and 2) store model results at the end of a tidal cycle for ease of comparing results. This harmonic tide was purposely set to propagate slowly in the seaward part by setting the phase difference to 3 degrees. Increasing the phase difference resulted in unrealistic high velocities in the seaward part of the model. These high currents resulted in an unstable model result; i.e. unrealistic bathymetrical changes. Another measure taken to prevent such unrealistic bathymetrical changes is by setting the Western seaward boundary as a closed boundary. Currents simulated along this closed boundary will have the same direction as the velocities at either the Northern or the Southern seaward boundary.

Waves are generated at the seaward boundary to propagate towards the estuary. Table 3 also summarizes the values which had been adjusted to simulate waves in the model. The wave conditions at the boundary needed to be specified in order to have the model do calculations in the seaward part of the model. Only one wave period was selected at the seaward boundary; the wave period was 6 seconds (or wave frequency of approx. 0.16 Hz). Therefore only a frequency space had been modeled although a frequency space between 0.05 and 1 Hz only had been selected. Furthermore, the wave direction at the boundary was set to 0 degrees with directional spreading of 4 degrees. A wave direction of 0 degrees indicates that waves propagate from the westward boundary to the estuary in the model.

The model in this study was run with a closed West seaward boundary. The Delft3D modeling software does not properly model waves on a closed boundary. Therefore, the results were not appropriately simulated. This led to simulation results with a smaller wave height than had been expected.

Upstream river discharge contributes to seaward transport of sediment (Guo et al., 2014). In this study non-cohesive sediment, i.e. sand, is transported by the upstream river discharge towards the seaward part. For reaching the objectives of this study cohesive sediment influx through the Northern seaward end is simulated in the model (Figure 8).

At the seaward part the suspended cohesive sediment concentration was set to 0.05 kg/m3. Such suspended sediment concentration can be found in the coastal part of the Amazon – Orinoco coast (Gensac et al., 2015).

Table 3: Boundary Conditions for generating Tides, Waves, and Suspended Sediment Concentration

Tides	
Oscillating frequency of harmonic tide:	30 deg/h
Tidal amplitude:	1.5 meter
Phase difference between Northern end and Southern end of seaward part:	3 degrees
Wave conditions at boundary:	
Peak period at offshore boundary:	6 seconds
Significant wave height at offshore boundary:	4 meters
Wave direction at offshore boundary:	0 degrees
Directional spreading at offshore boundary:	4 degrees
Orientation (Boundary from which waves originate)	West
Wave spectrum at boundary:	
Directional space	Between 359 – 360 degrees
Frequency space	Between 0.05 – 1 Hz
Number of frequency bins	24
Influx concentration of suspended cohesive sediment:	0.05 kg/m3
Total upstream river discharge:	23.11 m3/s

3.3 Analyzing Model Outputs

Several estuary characteristics of estuary morphology have been used by various scientists to link estuary morphological changes to different hydrodynamic and sediment dynamic conditions. Some morphological characteristics used in current research are: length-scale of width convergence, length-scale of depth convergence, and surface area of tidal flats (Townend, 2010, 2012; Edmonds & Slingerland, 2010; Van Dijk et al., 2013; Caldwell & Edmonds, 2014; Lanzoni & D'Alpaos, 2014). A method to determine morphodynamic equilibrium within an estuary is Energy Dissipation (Rodríguez-Iturbe et al., 1992; Van der Wegen et al., 2008). The following sections further elaborate on estuary characteristics that will be studied: 1) Tidal prism, 2) channel width and bed level, 3) Channel bank position, and 4) energy dissipation. These characteristics will be used in this study to reveal changes in estuary morphology in the model.

3.3.1 Tidal Prism

Tidal prism (the volume of water exchanged between an estuary and an adjacent sea during one tidal cycle) is related to Cross-sectional area of an estuary (Hume., 2005). An increase in tidal prism results in an increase of estuarine channel cross-section (Hume, 2005). This relation between estuary channel cross-section and tidal prism is as follow:

$$A = c * \Omega^n \qquad eq.\ 2$$

A => Channel cross-sectional area; c, n => are constants; Ω => tidal prism

Tidal prism (Ω) for the estuary is calculated as follow:

$$\Omega = \int_{LWS}^{HWS} Q(0,t)\,dt \qquad eq.3$$

HWS => High Water Slack; LWS => Low Water Slack; Q (0,t) => discharge at estuary mouth; t => time

Changes in tidal prism can be dictated by changes in estuary volume assuming all other hydrodynamic factors remain constant (Townend, 2010; Savenije, 2012). However, this formula does not reveal the shape of an estuary. Additional formulas for converging channel width and depth are needed.

In this study discharge was calculated at the estuary inlet to determine the volume of water entered. Furthermore, tidal prism was also used to compare changes in estuary morphology during a full tidal cycle. However, model data for each tidal cycle would consume storage volume. Therefore, only three randomly selected points during the simulation contained discharge data for a full tidal cycle.

3.3.2 Estuary Width and Depth Length-Scales Calculations

Estuarine channel width and depth are assumed to be exponentially decreasing from the estuary mouth to the landward end of an estuary (Townend, 2010). This degree of channel convergence corresponds to estuaries which have a zero gradient in water level and zero gradient in flow velocity (Savenije, 2012; Townend, 2012). Width and depth measurements are taken at mean tide level. The upper boundary of the channel is at mean tide level (Townend, 2010). These formulas for converging width and water depth at mean tide level are formulated as follow (Savenije, 2012; Townend, 2012):

$$W(x) = W_m exp\left(\frac{-x}{L_w}\right) \qquad \text{eq. 4}$$

$$h_s = h_m exp\left(\frac{-x}{L_h}\right). \qquad \text{eq.5}$$

W_m => the width of the channel inlet; h_{sm} => depth of the channel inlet; L_w^{-1} => the e-folding length scales of channel width; L_h^{-1} => e-folding length scales of channel depth.

Length scales of width (L_W) and depth (L_h) had been used to illustrate changes in the degree of channel width and depth convergence. Changes in these degrees take place during passage of tidal cycles. An increase in L_W indicates that the distance required for change in channel width increases. While a decrease in L_W illustrates that the distance required for a change in channel width also decreases. However, an L_W of 0 implies no channel width convergence (Friedrichs, 2010 in: Valle-Levinson, 2010; Townend, 2010; Pittaluga et al., 2015). The same goes for length scales of estuary depth; i.e. a higher value for L_h implies that the channel depth does not decrease at a high rate.

Both equation 4 and 5 were fitted on the model data results to calculate the length scales of width (L_W) and depth (L_h) for each time-series of data. The width and depth from the estuary mouth up to the fluvial end were used to calculate L_W and L_h. The reference for estuary depth was mean sea level. An exponential function can only fit on positive values. Therefore, the reference level was increased with 3 m to in order to get only positive values. Then an exponential function was linear fitted on the depth values to retrieve depth length scale values. The depth values were converted back to negative values by multiplication by a factor of -1.

Equation 4 and 5 represent an initial estuary and do not consider time varying estuary width due to tidal flats. Tidal flats can result in an increase of estuary width and in turn increase ebb tidal currents (Friedrichs, 2010 in: Valle-Levinson, 2010). However, various studies are still experimenting how to scale tidal flat width to estuary geometrics (Townend, 2012; Mariotti & Fagherazzi, 2013; Lanzoni & D'Alpaos, 2014). In this study tidal flats will be simulated within an estuary in which the initial estuary width is constant throughout a tidal cycle. Only through sediment deposition and channel bank erosion can tidal flats be formed.

3.2.3 Tidal Flat Width

Tidal flat width is regarded as the horizontal distance along a tidal flat cross-shore profile between high water and low water (Friedrichs, 2011). This description of tidal flats is also used in this study. Between high water and low water sedimentation or erosion takes place, therefore tidal flat can become wider or narrower (Friedrichs & Aubrey, 1995; Roberts et al. 2000; Pritchard et al. 2002; Pritchard & Hoggs, 2003; Bearman et al., 2010; Friedrichs, 2011). The tidal flat width will be normalized with total estuary width to compare the variations along the modeled estuary.

Tidal mudflats are distinguished from the sand flats on the basis of cohesive sediment deposits. Delft3d numerical modeling software classifies sediment as cohesive when mud fraction is above 0.3 for mixed sand and mud sediment (Deltares, 2012). This threshold mud fraction reflects the threshold at which the erosion velocity of cohesive sediment deviates from the erosion velocity of sand (Deltares, 2012).

Theories on tidal mudflat morphodynamic equilibrium focus on tidal flat width (Friedrichs & Aubrey, 1995; Roberts et al. 2000; Pritchard et al. 2002; Pritchard & Hoggs, 2003; Bearman et al., 2010; Friedrichs, 2011). Therefore, tidal flat width will be described in this study. Intertidal area on the other hand can later be used to describe the hypsometry of intertidal flats within an estuary (Moore et al., 2008). The area of intertidal flats can therefore be related to total estuary area. However, the focus in this study is on tidal mudflat width and intertidal area will only be mentioned briefly. Tidal mudflat width in model results had been measured with the aid of water level data in the model. Every grid cell between high and low water were regarded as tidal flats. Each grid cell contains one x- and y-coordinate. The grid cells between high and low water were used to calculate tidal mudflat width by subtracting y-coordinates of low water from the y-coordinates of high water. Some tidal mudflats that consisted of only one grid cell contained one y-coordinate for both low water and high water. Therefore, such tidal mudflats had a width of 0m.

3.2.4 Channel Bank Positions

Channel bank erosion resistance increases when composed out of cohesive sediment (Van Dijk et al., 2013). Increased erosion resistance by cohesive sediment may also be applied for tidal channel. Compared to fluvial conditions cohesive sediment can form tidal mudflats instead (Friedrichs, 2011). The extend of these mudflats simulated in this study will be disclosed by a graph illustrating mudflat area along a channel. It is expected that the extend of mudflats should expand by increasing cohesive sediment influx. However, migrating channels can erode channel banks (Van Dijk et al., 2013). Graphs showing cross-section of channel bed elevation and the amount of cohesive sediment present will be used to illustrate the migrating channel bed.

3.2.5 Energy Dissipation

Establishing estuary morphodynamic equilibrium which included channel-shoal pattern has been studied by Van der Wegen et al. (2008). Energy dissipation has been used by Van der Wegen et al. (2008) to illustrate the major effects in the overall channel morphology due to channel-shoal pattern. Long-term channel-shoal pattern reaching equilibrium will result in a decrease of energy dissipation (van der Wegen et al., 2008).

The energy dissipation equation has been rewritten by Van der Wegen et al. (2008) which has been derived from the original forumula by Rodríguez-Iturbe et al. (1992) for numerical simulation results given in grid cells. The modified energy dissipation formula by Van der Wegen et al.(2008) is as follow:

$$P_{cell} = \left[g \frac{n^2}{\sqrt[3]{h}} \rho_{w(\bar{u}^2+\bar{v}^2)^{1.5}+(\rho_s-\rho_w)g(S_x^2+S_Y^2)^{0.5}} \right] dxdy \qquad eq.6$$

In which:

g (gravitational acceleration [m/s^2]) = 9.81   n (Manning coefficient [sm$^{-1/3}$]) = 0.026

ρ_w (water density [kg/m^3]) = 1000 ρ_s (sediment density [kg/m^3]) = 2650

dx is distance between x-grid points (m)   dy is distance between y-grid points (m)

 h is water depth [m]   u is flow velocity in u-direction [m/s]

 v is flow velocity in v-direction [m/s] S_x is sediment transport in x-direction [m^3/ms]

 S_y is sediment transport in y-direction [m^3/ms]

However equation 6 contains the Manning coefficient while the numerical model assumes a constant. Thus equation 6 will be rewritten with the Chezy coefficient, eq. 8. First the Manning equation (eq. 7) was reformulated in terms of Chezy coefficient. The reformulated equation can be seen in equation 9. Next the energy dissipation provided by Van der Wegen et al. (2008) was rewritten with the Chezy coefficient (eq. 10). The Chezy coefficient in this study was set to 50.

$$n = h^{1/6}\sqrt{\frac{f}{8g}} \quad eq.7$$

$$C = \sqrt{\frac{8g}{f}} \quad eq.8$$

$$n = h^{1/6}\sqrt{\frac{1}{(C_u^2 + C_v^2)}} \quad eq.9$$

$$P_{cell} = \left[g \frac{1}{(C_u^2 + C_v^2)} \rho_{w(\bar{u}^2+\bar{v}^2)^{1.5}} + (\rho_s - \rho_w)g(S_X^2 + S_Y^2)^{0.5} \right] dxdy \quad eq.10$$

The energy dissipation formula applied by Van der Wegen et al. (2008) was used for an estuary with a closed upstream end. Therefore, the estuary was only forced by tidal currents. Hence, sediment transport took place by tidal currents. In this study fluvial discharge has been taken into account in the model simulations. In this case sediment is transport by fluvial and tidal currents during ebb phase of the tide.

In this study energy dissipation was first calculated for each cell (P_{cell}) and then integrated for the estuary and fluvial part. Each cell needed to be an active cell; an active cell is one in which velocity and sediment transport takes place. The energy dissipation calculated for the whole estuary and fluvial part also needed to be integrated over a tidal cycle (Van der Wegen et al., 2008). Energy dissipation was also calculated for the tide dominated part of the estuary. This was done to determine the effect of the tide dominated part in the energy dissipation. The method by Pittaluga et al. (2015) will be used to determine which part of the estuary will be taken as tide dominated part. Their method makes use of a tidal length to determine the tide dominated part in an estuary. Tidal length starts as the estuary mouth and ends where tidal amplitude is reduced to 5% of the tidal amplitude at the estuary mouth (Pittaluga et al., 2015). The position where sediment flux by tidal currents decreases by 50% is another option for choosing the end of the tidal length (Pittaluga et al., 2015). The transport of suspended cohesive sediment can also be driven by salinity circulation (Van Kessel et al., 2011). Salinity circulation has not been taken into account in this study. Therefore, the end of the tidal length was chosen at the location where the tidal amplitude is reduced by 5% of the tidal amplitude at the estuary mouth.

4 Results

The previously described model produced estuaries with tidal flat, and shoals. Tidal flats were composed of sand or cohesive sediment (mud). Only when marine cohesive sediment influx is present will a tidal mudflat form. Another result produced by the model is a spatial difference in tidal flat width along the estuary. Tidal flat width along the estuary shows a trend which starts narrow at the estuary mouth, widens further upstream, and narrows near the end of the estuary. The model also showed shoals form on the channel bed when either sand influx was present or when both marine cohesive sediment and sand influx were present. Between these shoals a lower elevated part is present in which channels flow. An overall trend of estuary morphological evolution will first be presented in the next section followed by an analysis of tidal flats, channel bank position and estuary morphodynamic equilibrium.

4.1 Estuary Morphodynamic Model Results

General morphological trends that were observed in the estuary model results were: 1) a relatively greater widening of estuary width when only fluvial sand influx was present, and 2) a relatively lower widening of estuary width when both fluvial sand and marine cohesive sediment influx was present. The net morphological changes in these trends take place after each tidal cycle. Therefore, each morphological is given in Figure 9 with respect to number of tidal cycles. The morphological evolution of the morphological trends can be seen in Figure 9.

Tides and waves were the hydrodynamic forces to induce morphological trends in Figure 9. However, only waves were used in two morphodynamic simulations (Figure 9 a1 to d1, and 9 a3 to d3). The effect of waves was noticable in the simulations with marine cohesive sediment influx. Waves kept marine cohesive sediment from depositing in front of the estuary and likely on the tidal flats near the estuary mouth. Therefore, the coastal part did not accrete a high rate (Figure 9 a3 to d3) compared to the simulation where only tides were present (Figure 9 a2 to d2).

Shoals and channels had appeared in all model results in which the simulations started from a flat sloping bed (Figure 9). In each simulation can be seen that shoals are relatively small in the early stages (Figure 9 a, a1, a2, and a3) and increase in size with increasing number of tidal cycles (Figure 9). These shoals are formed along with deepening of channels which indicate a relatively high amount of sediment transport within the estuary.

Figure 10 illustrates quantitative morphological and hydrodynamic results which will be used to aid in forming a conclusion of morphodynamic equilibrium. Further detail on morphodynamic equilibrium is given in section 4.4. Panels i, ii, and iii in Figure 10 show respectively estuary bed elevation, estuary width, and plan area of intertidal area. A difference is noticeable in estuary width of all simulations. The estuary width are closer to the initial estuary width for simulations

with cohesive sediment influx. In these cases tidal areas composed of cohesive sediment (mud) also form along the channel banks (Figure 10 panels ii, and iii). For the simulations in which only sand was present the estuary width was further away from the initial estuary width. Tidal flat area in this case were not composed of mud. These estuary morphological features might be in morphodynamic equilibrium. The tidal currents and tidal range might suggest this. The current velocity amplitude (Figure 10 panel v) in both ebb- and flood-direction are similar in the estuary part up to about 7 km upstream of the estuary mouth. The tidal range (Figure 10 panel iv) seems constant to about 7 km upstream of the estuary mouth. Further upstream the tidal velocities and tidal range decreases due to increased bed elevation and influence of fluvial discharge.
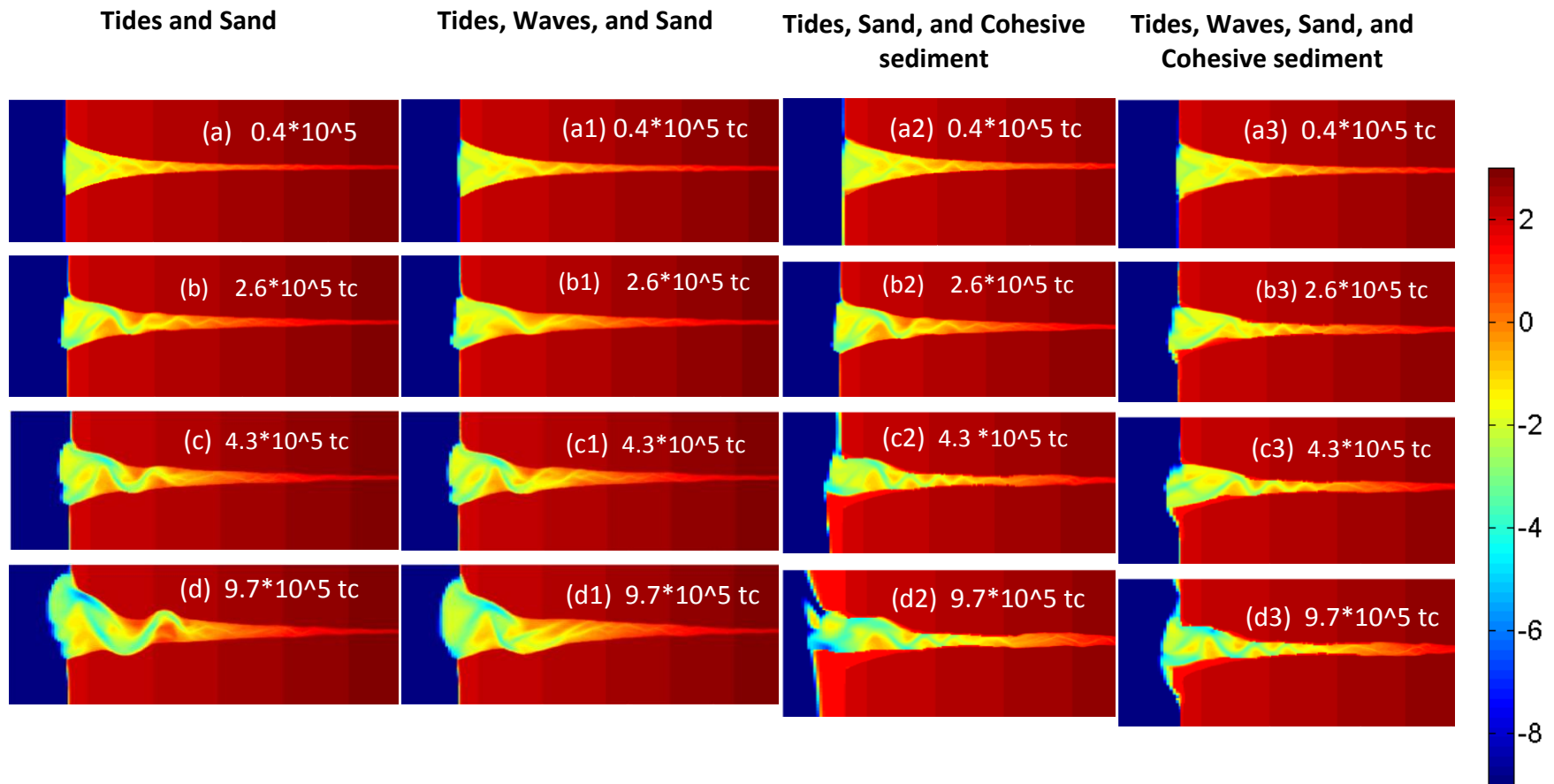
Figure 9: Bed level evolution with combinations of tides waves upstream sand influx and marine cohesive sediment influx. "tc" stands for tidal cycles.
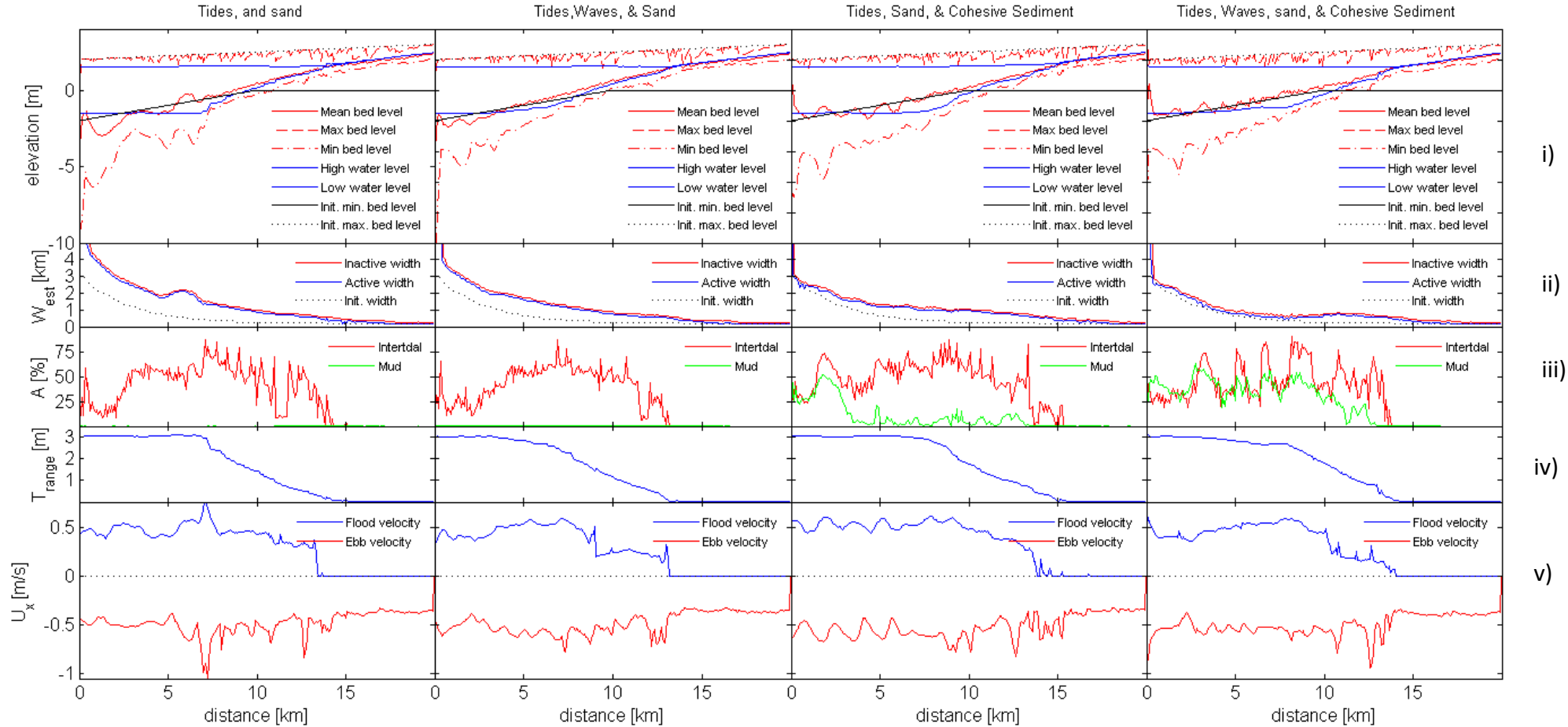
Figure 10: Estuary morphology characteristics at the end of each simulation. All panels illustrate parameter values in alongshore direction from the estuary mouth to the head of the estuary. On the abscissa of each panel the distance starting from the estuary mouth towards the landward end are illustrated. The parameter on the ordinate of each panel are as follow: cross shore average bed elevation (elevation) estuary width (W_est) intertidal area in percentages (percentages are taken relative to total active cells along cross-section of the estuary; this is separately for intertidal area composed of non cohesive and cohesive sediment. Active cells are referred to computational grid cells that participate in morphodynamic simulations) tidal range (T_range) and velocity amplitude in x-direction (Ux).

4.1.1 Length Scale of Estuary Width

Model results in this study showed that length scales of width are relatively larger for estuaries simulated without cohesive sediment than for estuaries simulated with cohesive sediment (Figure 12). The graphs also indicate the trend of the length scale of estuary width evolution. However, between the two results with cohesive sediment influx a difference was observed when waves were added to the model. The simulation without waves resulted in a higher length scale of width compared to the simulation without waves. Such higher value indicates an estuary in which the width changes after a longer distance. Figure 9 a2 to d2 show the changes to an estuary bed level; small width convergence had developed when focused on the bathymetry lower than 2 meters. A reason for this higher values is due to the sedimentation at the estuary mouth. This higher sedimentation can be seen in Figure 10 panel iii of the simulations with only cohesive sediment (mud). Therefore, the width at the estuary mouth decreases. Length scales of width seems to stabilize for model results with waves and mud (Figure 12). The values for the length scales are smaller compared to the simulation without waves. The bathymetry of the simulation with waves and mud indicates that less sedimentation took place near the estuary mouth (Figure 9 a3 to d3). Wave heights were not properly modeled to the desired wave height, but were sufficient to prevent sediment deposition in the estuary mouth. Therefore, mud was kept in suspension and transported further upstream of the estuary by tidal currents. As a result suspended mud concentration increased further upstream. An increase of upstream intertidal areas composed of mud reflect increased suspended sediment concentration (Figure 10 panel iii of the simulation with waves and mud).

Model results without suspended mud influx show a nearly stabilizing trend for the length scale of width (Figure 12). This indicates that the estuary shore will not change rapidly. A reason can be a nearly constant tidal range and velocity amplitude from the estuary mouth to about 7 km upstream of the estuary (Figure 10 panel iv and v). A nearly constant tidal range and velocity amplitude implies that the net sediment transport is reduced. Therefore, morphological changes can take place at a low rate. A small difference in length scales was observed between simulations with and without waves. Wave heights were not properly modeled which did not contribute to significant morphological changes.

4.1.2 Length Scale of Estuary Depth

Every simulation results showed that the channel bed elevation near the mouth of the estuary decreased relative to the initial bed elevation (Figure 9 and 10i). Figure 10i illustrates that the channel bed elevation within the estuary changed within short distances. These changes in channel bed elevation are reflected in the length scales of channel depth (Figure 13). Changes in length scale of channel depth needed to take place due to changes in length scale of channel width by either intertidal area forming or erosion of channel banks. Changes in length scale of channel bed were found to start stabilizing at approximately 2*10^5 tidal cycles (Figure 13).

The model results showed a lower length scale of channel depth for the simulations without mud influx. This indicates that channel bed elevation increases within a short distance; i.e. the channel becomes shallower at a greater rate towards the head of the estuary. These changes in channel bed elevation was needed to balance changes in channel width to achieve a low gradient in alongshore flow velocity and tidal range. Figure 10 panel iv and v illustrate the nearly constant tidal ranges and velocity amplitudes up to about 7 km upstream of the estuary mouth. However, as the channel bed elevation becomes higher than low water level the tidal range decreases. Fluvial discharge becomes more dominant after this point.

The length scales of channel depth showed a higher value for the simulations with cohesive sediment (Figure 13). Therefore, channel depth decreases less when compared to the simulations without cohesive sediment influx. The higher values of length scale of channel depth are balanced by lower values of length scales of channel width. As mentioned in the previous section tidal flats formation resulted in a decrease of the length scale of channel width.

4.1.3 Tidal prism

Tidal prism had shown an increase for each of the simulations. Along with changes in length scale of estuary width and depth do the tidal prisms change. The time when tidal prism starts to stabilize is approximately similar to the time when the length scales also start to stabilize. The model results illustrated that the tidal prisms for the simulations with mud influx tend to stabilize at lower tidal prism compared to the simulations without mud influx. Figure 11 shows the model results obtained for each simulation.

The tidal prism for simulations with mud influx show a smaller tidal prism. The simulations with mud influx reached a stable length scales of width and depth at an earlier stage compared to the simulations without mud influx (Figures 12 and 13). Tidal amplitude and propagation phase had been constant during all model runs. Therefore, tidal prisms only changed due to morphological changes. Although the length scale of width increased rapidly for the simulation with only mud influx, the tidal prism was lower than tidal prism of the simulations without mud influx. From these results can be seen that marine cohesive sediment influx affects morphological evolution of estuaries.
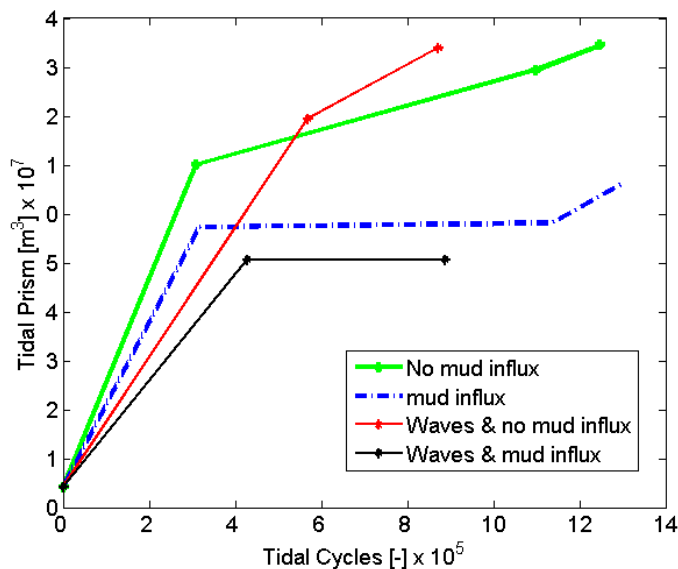

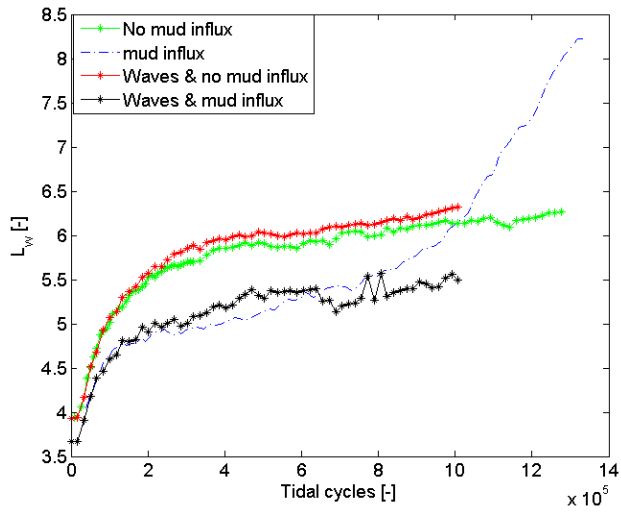**Figure 11: Changes in tidal prism with respect to time (tidal cycles).**

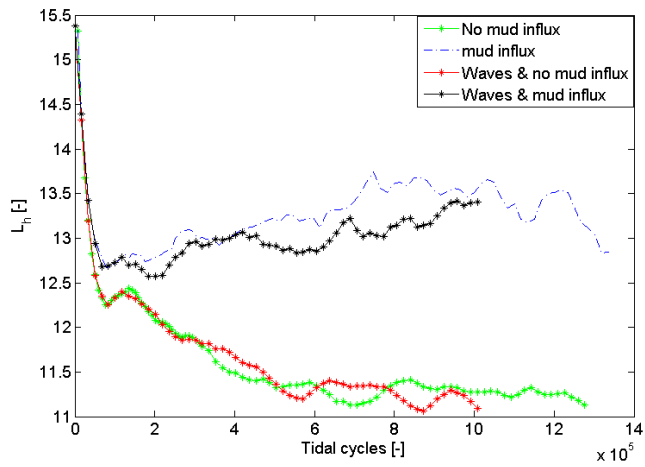**Figure 12: Length scale of width for all four simulations.**

Figure 13: Length scales of channel depth (L_h) as function of tidal cycles

4.2 Tidal Flat Width and Cohesive Sediment Deposits

The model results illustrated an alongshore spatial variation of tidal mudflat width which was generally wide at the estuary mouth and narrow at the estuary head. The intertidal mudflat area showed similar results. This difference in mudflat width was attributed to spatial difference in suspended load transport along an estuary.

The simulations with marine cohesive sediment influx showed the spatial difference in mudflat width to occur where mud deposition is greatest. Figure 14 and 15 illustrate locations of mud deposits within the models with mud influx. Figure 14 shows the simulations with only mud influx while Figure 15 the simulations with waves and mud influx. The initial condition of the estuary had no mud deposits and has been increasing with the number of tidal cycles. Deposition of mud has also been observed in the seaward part of the model that was modeled with only mud influx (Figure 14). However, there was less mud deposition in the seaward part when the simulation was done with waves and mud influx (Figure 15). Waves have prevented mud deposition in the seaward part of the estuary which in turn can lead to more mud transport into the estuary by tidal currents.
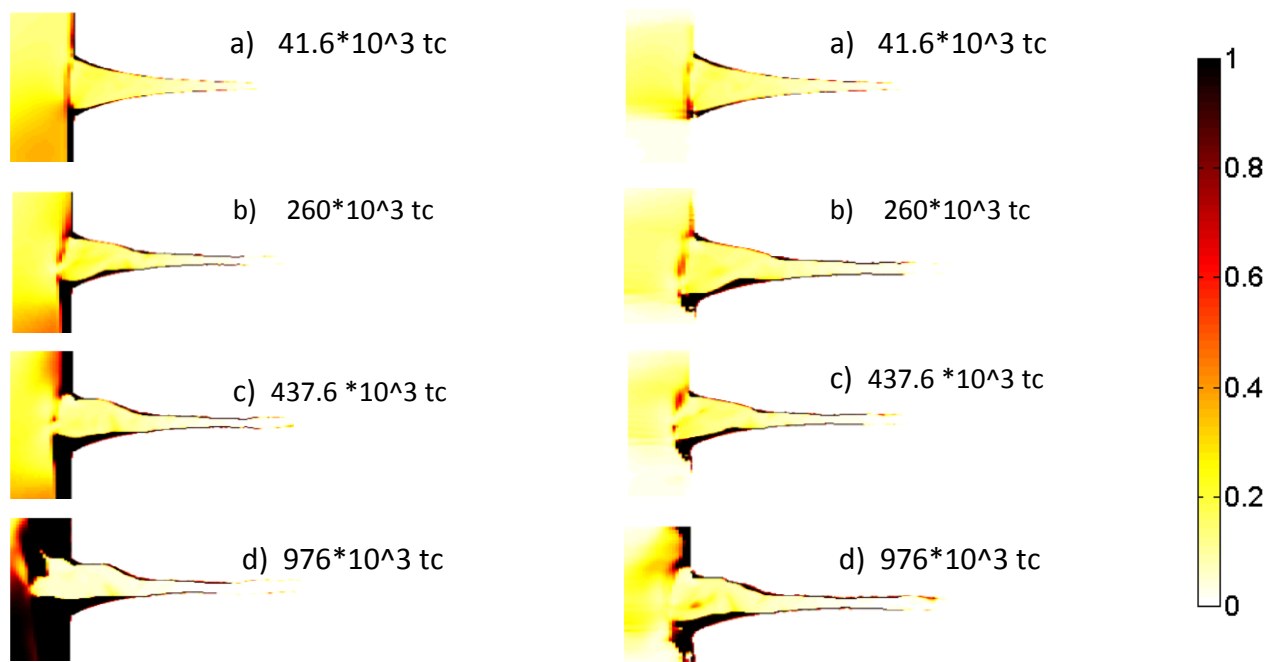
Figure 14: Cohesive sediment deposits in top layer for simulation with only mud influx. Each simulation time is represented by tidal cycles (tc). Sediment transport was modeled with only tidal currents. The simulation illustrates cohesive sediment deposits along channel banks and in front of the estuary.

Figure 15: Cohesive sediment deposits for simulation with mud influx and waves. Both this simulation and a20b show an increase in deposits near the tidal mouth. The color bar scale illustrate the sediment fractions between 0 to 1.

45

Intertidal areas composed of mud were only formed for the simulations with mud influx. Figure 10 panel iii shows these mud intertidal areas. These muddy intertidal areas contained mud which deposited from the suspended sediment brought in by the mud flux. The normalized width of the mud deposits for simulations with only mud influx, and both mud and waves are illustrated in Figure 16.

The normalized deposit widths are approximately the same near the estuary mouth, but further upstream the normalized width do not indicate deposits for the simulation with only mud influx. As was mentioned in section 3.2.3, the algorithm to analyze deposit width discarded these width values with the size of a grid cell or smaller. This indicates that the size of deposits upstream in the model with only mud influx had a width that was smaller than a grid cell size. Figure 16 shows the deposit width for simulations with mud influx. A relatively small upstream suspended load resulted in no mud deposition upstream (Figure 18 left panel).

Model runs that included waves and mud influx have resulted in upstream deposits which had a width larger than a grid cell (Figure 16). The width of these deposits coincide with the increased suspended load further upstream (Figure 18 right panel). Although waves were not properly modeled in the seaward part the bed shear stresses induced by these waves were sufficient to entrain mud which could deposit in front of the estuary. Tidal currents transported this entrained mud further upstream which increased the suspended load. Therefore, the simulations with wave and mud influx were able to result in upstream mud deposits.

Results also show wider tidal mudflat width at the estuary mouth and narrow tidal mudflats near the head of the estuary (Figure 17). The tidal mudflat width show the same trend as the mud deposits in Figure 16. The tidal mudflats are a result of mud deposition and therefore sensitive to suspended load transport. As more suspended load is transported upstream the wider tidal mudflats become.

Relatively small differences are observed between the width of the mud deposits and the tidal mudflats. Inactive points on the mud deposits was a reason for these small differences. Mud deposits with an elevation near high water level are regarded as an inactive point. As a result, high water is not modeled over the inactive points. Tidal flat width can therefore be smaller that the mud deposit width.
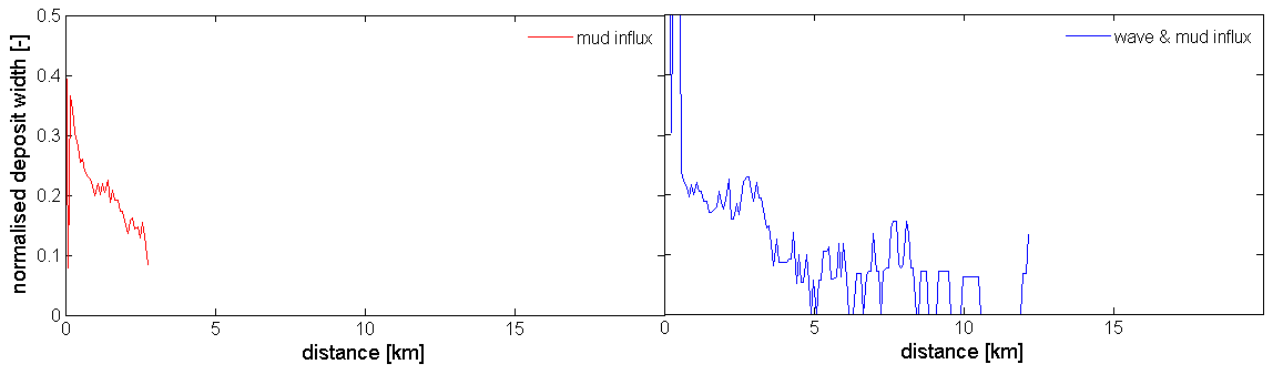
Figure 16: Mud deposit width along the estuary at the end of the simulation period. The deposit width was normalized with total estuary width.
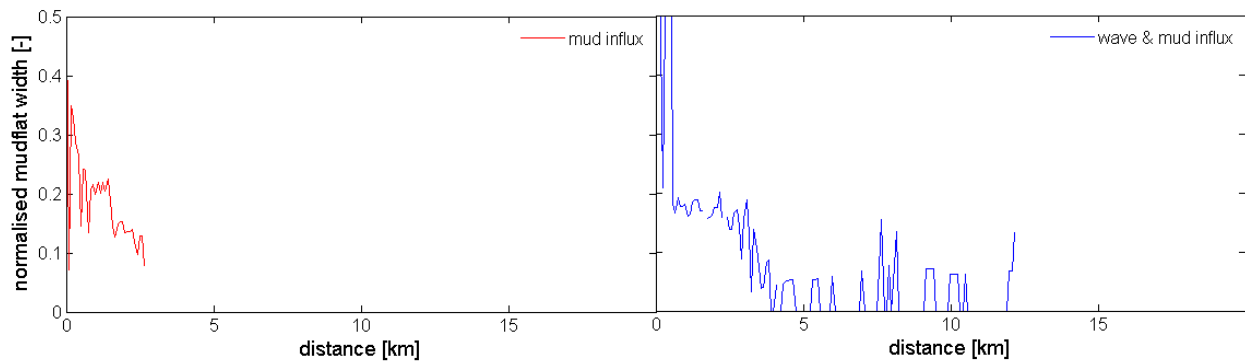
Figure 17: Normalized alongshore tidal mudflat width. The mudflat widths were normalized with total estuary width.
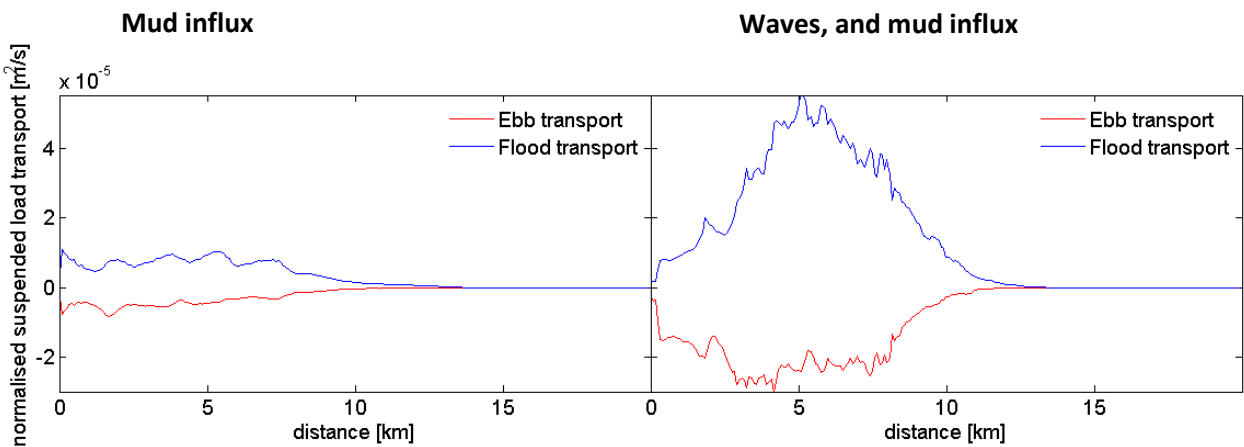
Figure 18: Suspended load transport along the estuary in the simulation. These values had been obtained at the end of each simulation. Suspended load transport is normalized with estuary width.

4.3 Channel Bank Position

Shoals forming on the channel bed and tidal flats have been observed in the model results. Channels follow the lowest contours set by these shoals. The flow of these channels can be deflected towards a channel bank resulting in local channel bank and tidal flat erosion. Deposition of sediment can take place on the shoals allowing for accretion of channel banks or tidal flats. Through such erosion lateral migration of channels take place. As a result the position of the channel bank migrates along with it.

Channels deflected to channel banks can cause a local erosion during low tide and high tide. This localized erosion is seen in all model results with tides, waves, sand and mud influx. During low tide water concentrates in the lowest channel bed between sand shoals, while during high tide water can flow over the sand shoals. Although water can flow over these sand shoals most of the bed shear stresses are still exerted in the lowest part of the channel. Figure 19 to 21 illustrates flow directions and locations of high bed shear stresses. The locations with high bed shear stresses have also been observed to move along during the tide. This might also contribute to localized erosion of channel banks and tidal flats.

Locations of channel migration at a cost of channel bank are illustrated in Figure 23 panels a to j. For the simulations without mud influx the channel migration takes place without channel bank accretion (Figure 23 panels a, d, and g). Sand transport only took place as bed load in the model. The bed shear stresses over the shoals were not sufficient to transport sand which did not result in channel bank accretion, but shoal accretion did take place. By adding mud influx to the model channel bank accretion was able to take place (Figure 23 panels b, and c). This indicates that the bed shear stresses above the shoals were sufficient to transport mud to the channel banks. Mud influx further upstream was likely balanced by channel bank erosion (Figure 23 panels e, f, h, and i). Channel migration and deepening did take place in Figure 23 panels e, f, h, and I, but not as significant to the simulations without mud influx.

Simulations with mud influx illustrated that mud was able to deposit on the channel bank before being eroded by lateral channel migration. Figure 23 panels a to d show mud deposition and the morphological evolution of a channel cross-section. At the channel bank where the channel migrates away from the channel bank can mud deposits increase in elevation. Once the mud deposit elevation increases above low water level can de mud deposit become a tidal flat. The opposite occurs at the channel bank where the channel is migrating towards to. The mud deposit formed before the channel migration is eroded and also the channel bank. This illustrates the local changes that takes place on tidal mudflat morphology.

Figure 19: Simulation done with tidal currents and only sand influx. Direction of velocity vectors and bed shear stress at low tide (panel a and c) and high tide (panel b and d). The upper panels are the bed level elevation with velocity vectors (black arrows). The lower panels indicate the bed shear stress caused by tidal currents. Cross-sections 60 (10.8 km upstream), 90 (13.3 km upstream), and 120 (15.8 km upstream) are shown in Figure 23. Blue arrows in a) and b) point to a sand shoal on the channel bed.
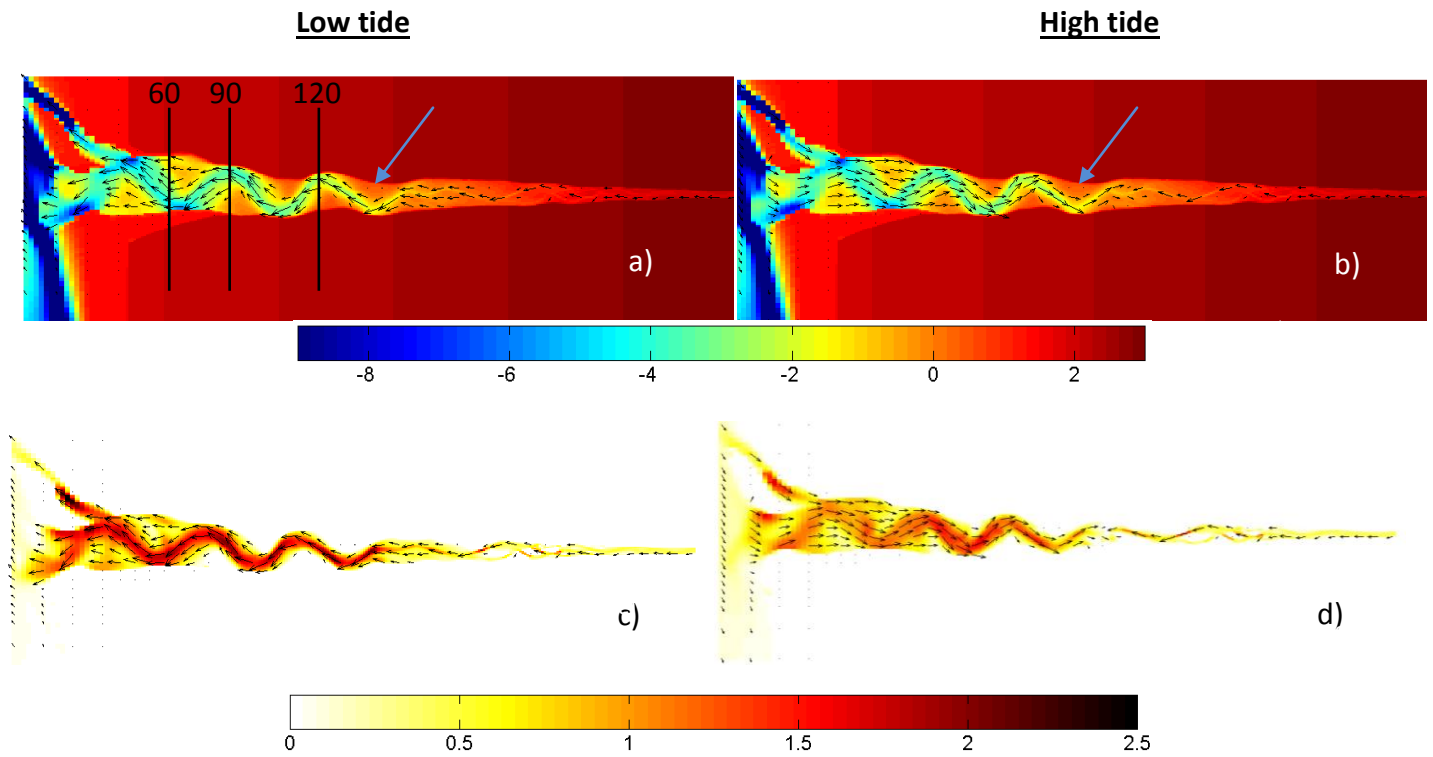
Low tide   **High tide**

Figure 20: Simulation done with tidal currents, sand, and mud influx. Direction of velocity vectors and bed shear stress at low tide (panel a and d) and high tide (panel b and d). The upper panels are the bed level elevation with velocity vectors (black arrows). The lower panels indicate the bed shear stress caused by tidal currents. Cross-sections 60 (10.8 km upstream), 90 (13.3 km upstream), and 120 (15.8 km upstream) are shown in Figure 23. Blue arrows in a) and b) point to a sand shoal on the channel bed.
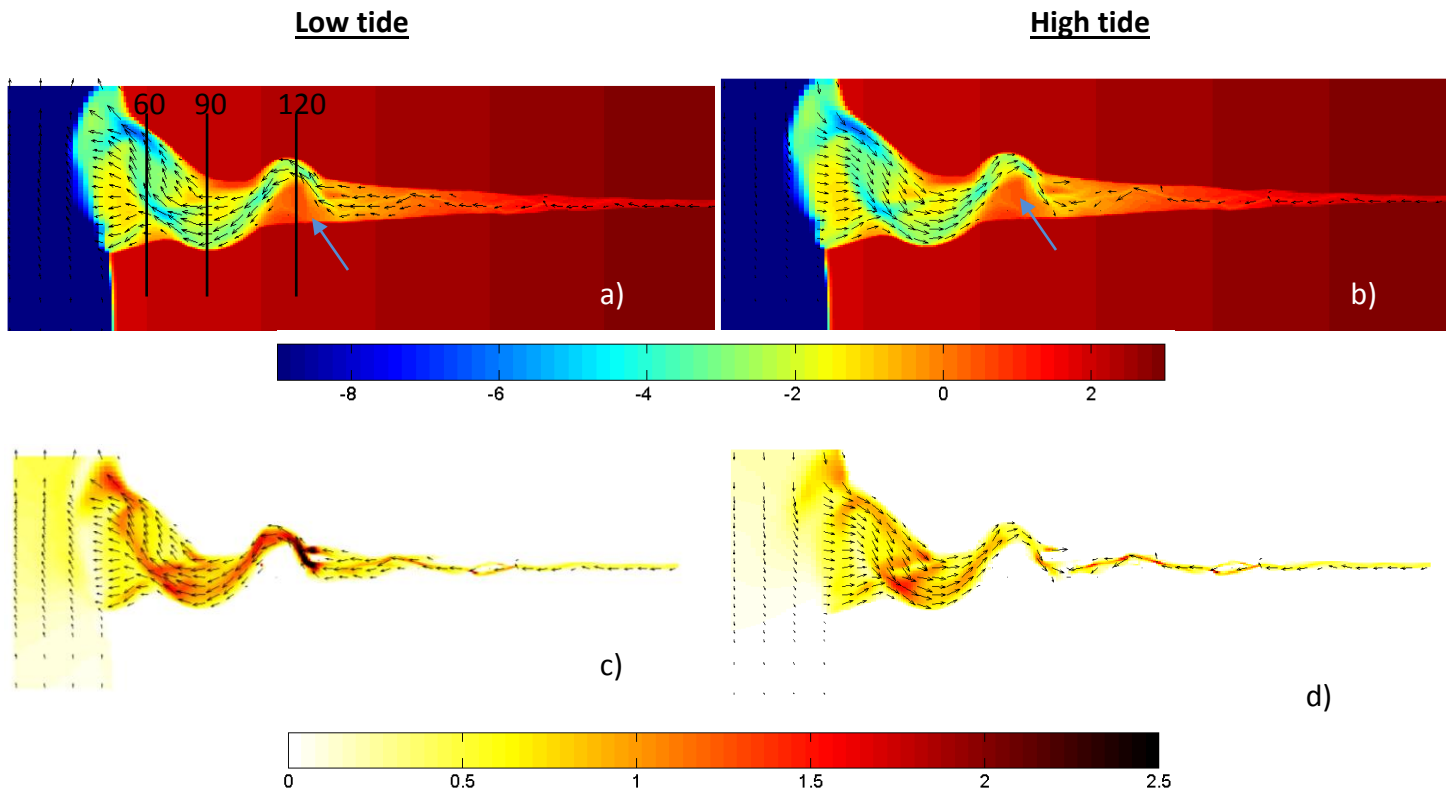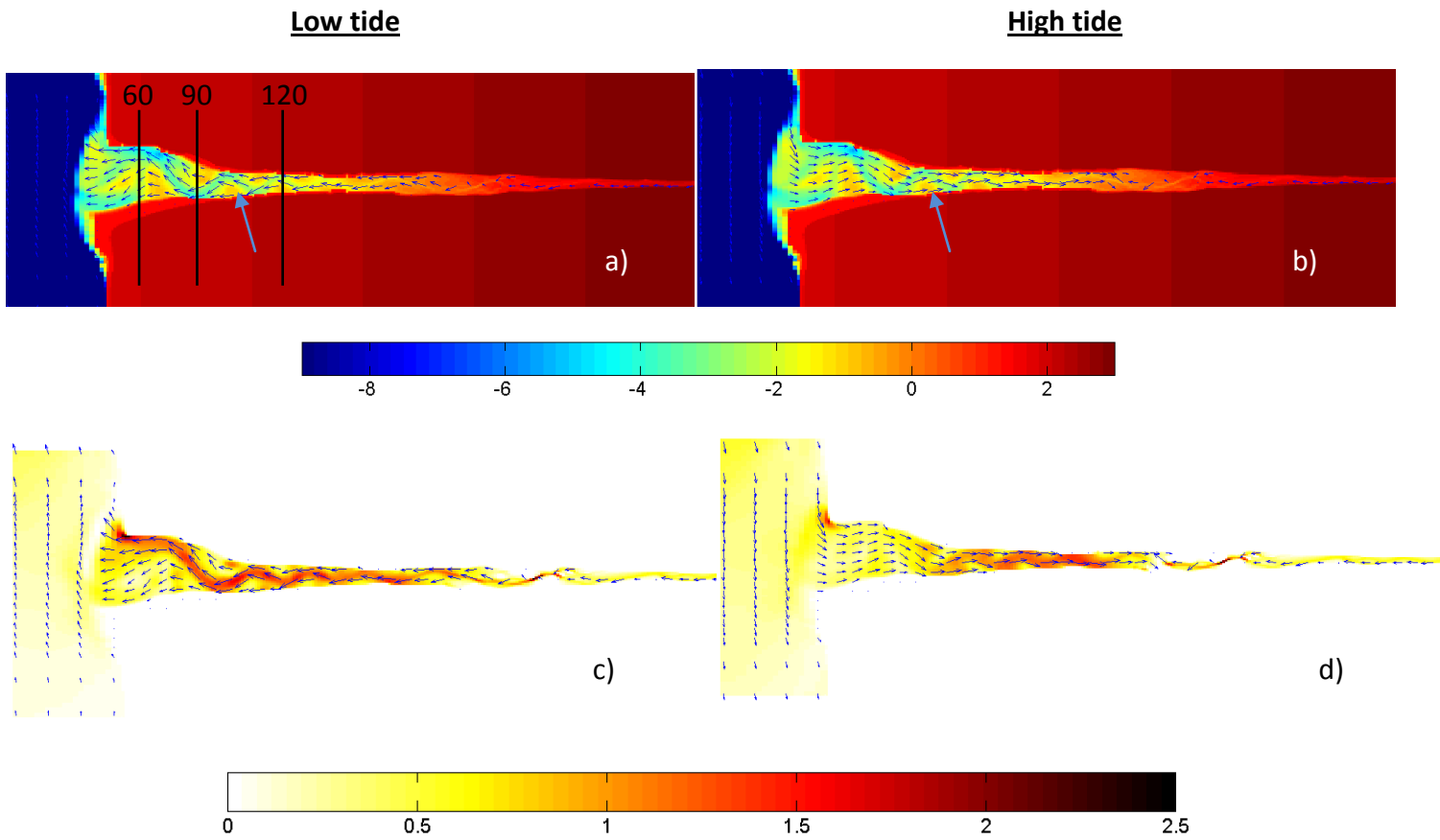
Figure 21: Simulation done with tides, waves, sand, and mud influx. Direction of velocity vectors and bed shear stress at low tide (panel a and d) and high tide (panel b and d). The upper panels are the bed level elevation with velocity vectors (black arrows). The lower panels indicate the bed shear stress caused by tidal currents. Cross-sections 60 (10.8 km upstream), 90 (13.3 km upstream), and 120 (15.8 km upstream) are shown in Figure 23. Blue arrows in a) and b) point to a sand shoal on the channel bed.

Tides and sand influx

Tides, sand and marine mud influx

Tides, waves, sand and marine mud influx

60

90

120

Cross section number

S   N   S   N   S   N

a)   b)   c)

d)   e)   f)

g)   h)   i)

—— 0 tc
—— 41.6*10^3 tc
—— 260*10^3 tc
—— 437.6*10^3 tc
—— 976*10^3 tc
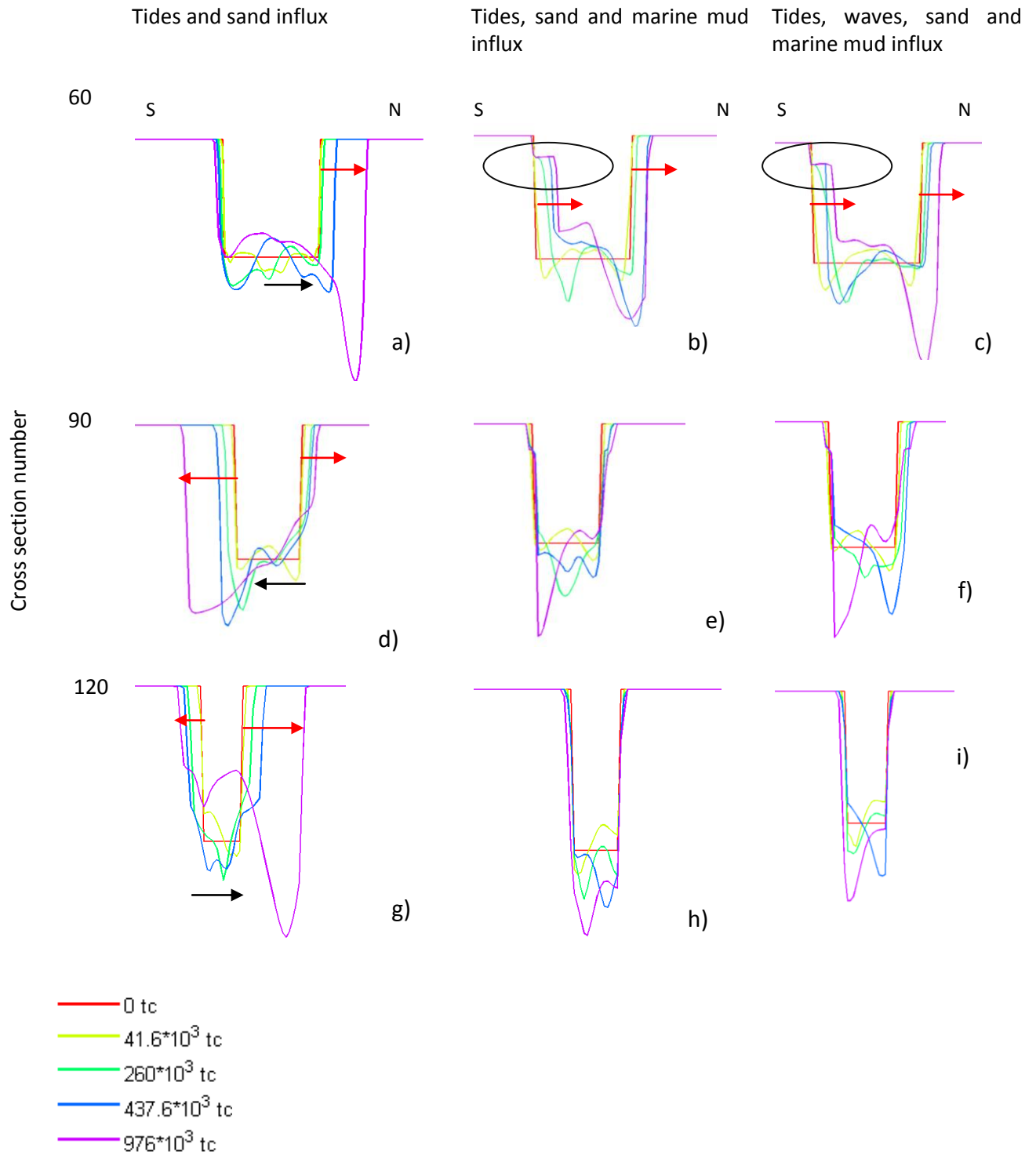
Figure 22: Channel position during evolution of estuary. The black arrows indicate channel position at the end of each simulation. The red arrows indicate the direction of channel bank migration. Channel bank position are referenced to channel bank position at 0 tidal cycles (tc). The black ellipses in panel b and c point to the tidal flats in the model results. More detail on tidal mudflat
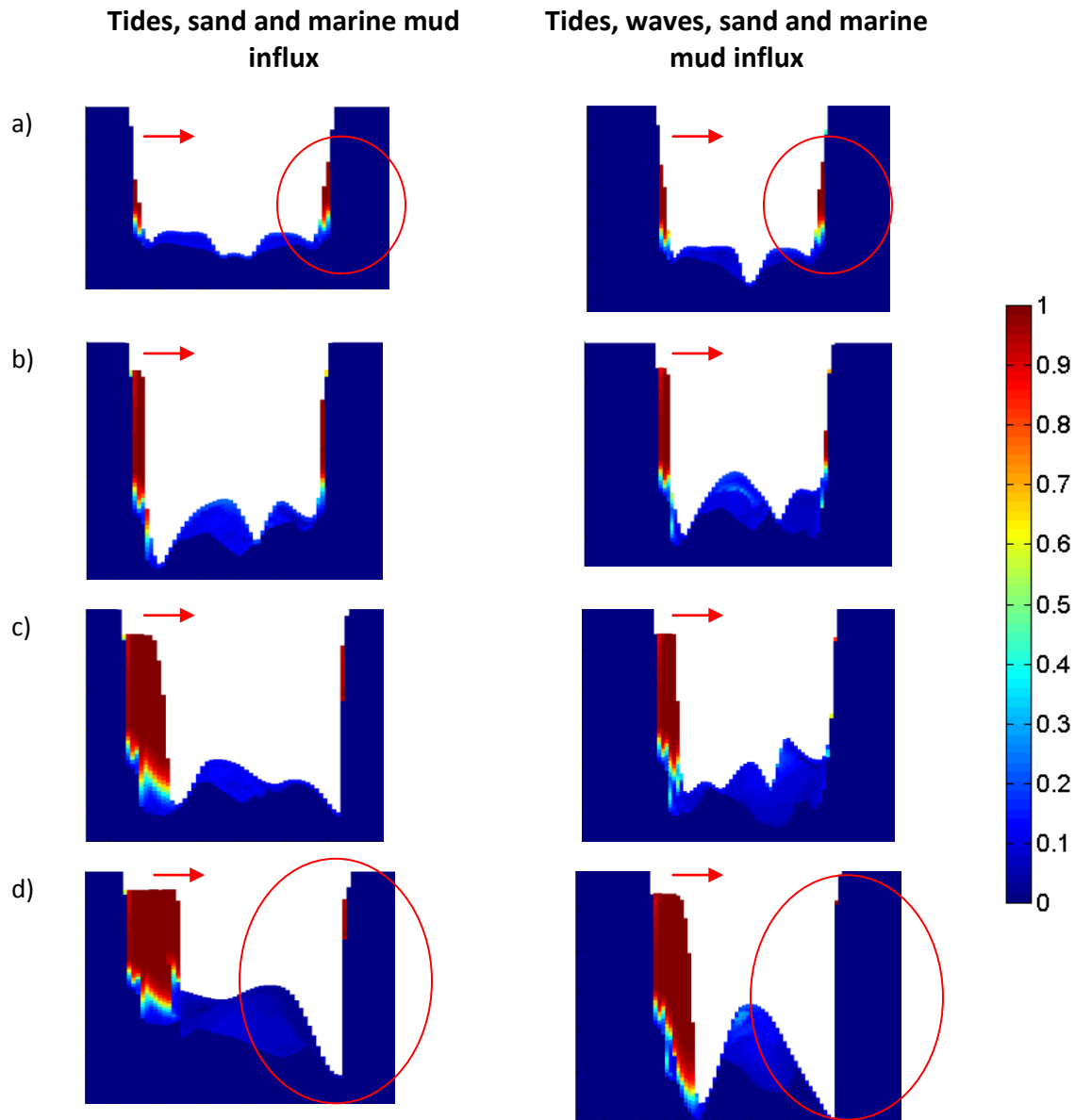
Figure 23: Morphological evolution of channel cross-section; accretion of tidal mudflat and channel migration takes place. Red arrows indicate the direction of mudflat accretion. The color scale bar illustrates the mud fraction in the mudlfats; the scale starts from a mud fraction of 0 to a mud fraction of 1. Tidal cycle are as follow a) 41.6*10^3, b) 260*10^3, c) 437.6*10^3, and d) 976*10^3 tidal cycles. The red ellipses illustrate the erosion of a mud deposit by channel migration.

4.4 Morphodynamic Equilibrium

Morphodynamic equilibrium based on energy dissipation indicated a difference between simulations with and without mud influx. The energy dissipation for simulations without mud influx were lower than the simulations with mud influx. The contribution of the fluvial part to energy dissipation have been significant to total energy dissipation for the estuary. Furthermore, energy dissipation showed a link with morphological changes to estuary width and depth length scales. Each simulation showed a relatively stable energy dissipation after approximately $2*10^5$ tidal cycles. This number of tidal cycles coincided with the time after which estuary length scales stabilized.

Energy dissipation stabilized at a higher value for the simulations with mud influx compared to simulations without mud influx. Figure 24 shows the energy dissipation between the simulations with and without mud influx. This relatively higher energy dissipation is caused by the contribution of mud fluxes to the sediment transport components (S_x and S_y) in the energy dissipation equation (eq. 10). Both the mud flux and the sand fluxes were taken together in the sediment transport components. Therefore increasing the energy dissipation. The simulations without mud influx only had sand influx into the estuary. This could have resulted in lower energy dissipation for the simulations without mud influx.

Energy dissipation calculated for combined estuarine and fluvial part (Figure 24) was higher than the energy dissipation of only the estuarine part (Figure 25). This difference in energy dissipation shows that fluvial sand influx or fluvial currents had contributed significantly. The morphological changes in the fluvial part likely stabilized after approximately $2*10^5$ tidal cycles.

The energy dissipation was calculated separately for the sand fluxes in the simulations that contained mud influx. Both the figures 24 and 25 show the energy dissipation for the separate sand fluxes (indicated in Figure 24 and 25 as 'Sand in comb. Sand & Cohesive sed.' and 'Wave, Sand in comb. Sand & Cohesive sed.'). The energy dissipation for the separate sand fluxes approximately follows the energy dissipation in the simulation without mud influx. However, an increase in energy dissipation was observed near the end of the simulations for the separate sand flux in the simulations with only mud influx. This increase was attributed to the changes in estuarine morphology.

Both the trend of the estuary width and depth length scales (Figures 12 and 13) concided with the trend of the energy dissipation in Figures 24 and 25. All four figures show a stabilizing trend after approximately $2*10^5$ tidal cycles. This coinciding trend is present due to the sediment transport that takes place in morphological changes. Of particular interest in the increased sand flux in the simulation with only mud influx in Figures 25 (indicated as 'Sand in comb. Sand & Cohesive sed.'). This sand flux increase near the end coincides with the increase in width length

scale of the simulation with mud influx. Furthermore, this sand flux also appears in Figure 25 which indicates that this increase can be attributed to tidal currents. The reasons for this increase could be due to shoals shifting or lateral channel migration. Also the energy dissipation fluctuating trend in the simulation with mud influx could be attributed to lateral channel migration. However, no further evidence has been found for linking the effect of lateral migrating channels on energy dissipation.
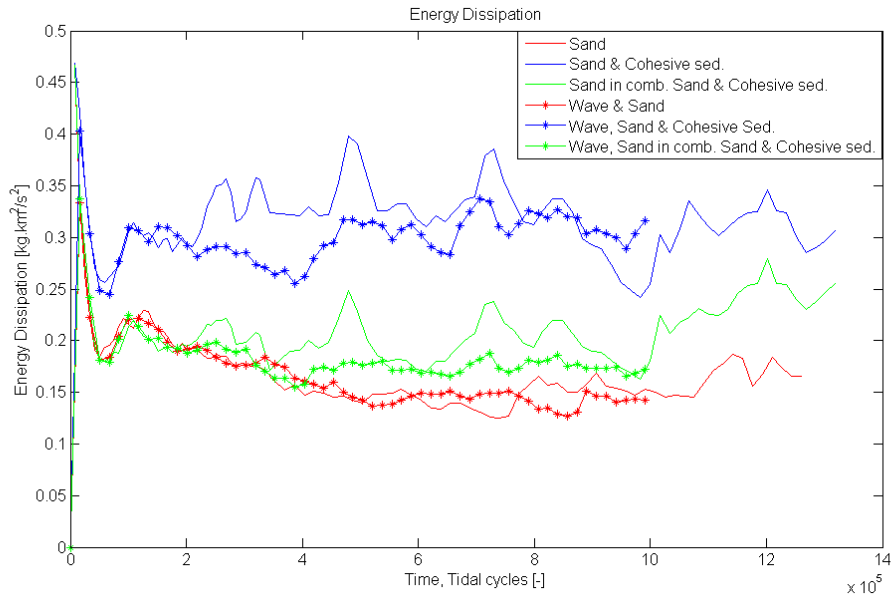
Figure 24: Energy dissipation along the estuary mouth to the river head. The main trend of the graph shows a slight increasing trend.
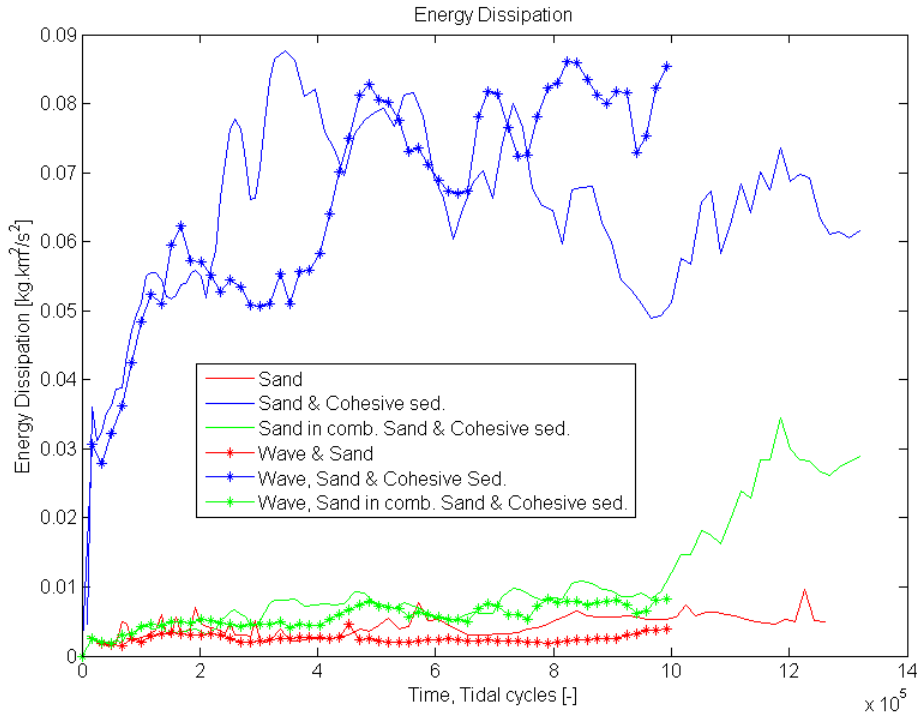
Figure 25: Energy Dissipation from estuary mouth (0 km) to near tidal limit (± 6 km). The approximate tidal limit distance was estimated on the basis of tidal ranges in Figure 10. In all simulations the tidal range remained approximately constant up to 6 km upstream.

4.5 Problems Encountered During Numerical Modeling

Previous model runs in this study encountered unrealistic morphological changes to either the estuary channel bathymetry or seaward bathymetry. These unrealistic morphological changes were: 1) rapid infilling of estuary by cohesive sediment, 2) sedimentation of cohesive sediment at the seaward boundary, 3) erosion of seaward bathymetry until the lower model limit was reached, and 4) shoal formation in the seaward part with elevation near mean sea level. Other limitations that remained during modeling were: 1) tidal currents alone did not prevent cohesive sediment from depositing in the coastal part of the model, and 2) wave heights could not be properly modeled on a closed seaward boundary.

Rapid infilling of the estuary with cohesive sediment (mud) was one of the model instabilities that was encountered. Marine influx in these models was placed at the western seaward boundary. The concentration of the mud influx was set at 0.05 kg/m^3. Tidal currents were generated by water level gradients at the seaward boundary which varied periodically with a M2 tidal component and an amplitude of 1.5 m. The northern and southern seaward boundaries were still modeled with an open boundary, but the water levels at the northern and southern boundaries were not varied by the M2 tidal component. Figure 26 b illustrates the

56

infilling of the estuary with cohesive sediment after 2.9*10^5 tidal cycles. As a result, the estuary bathymetry rose above mean sea level and only one main channel maintains. The location of mud deposits can be seen in Figure 26 c. Mud deposition occurred in both the seaward part and the estuary.
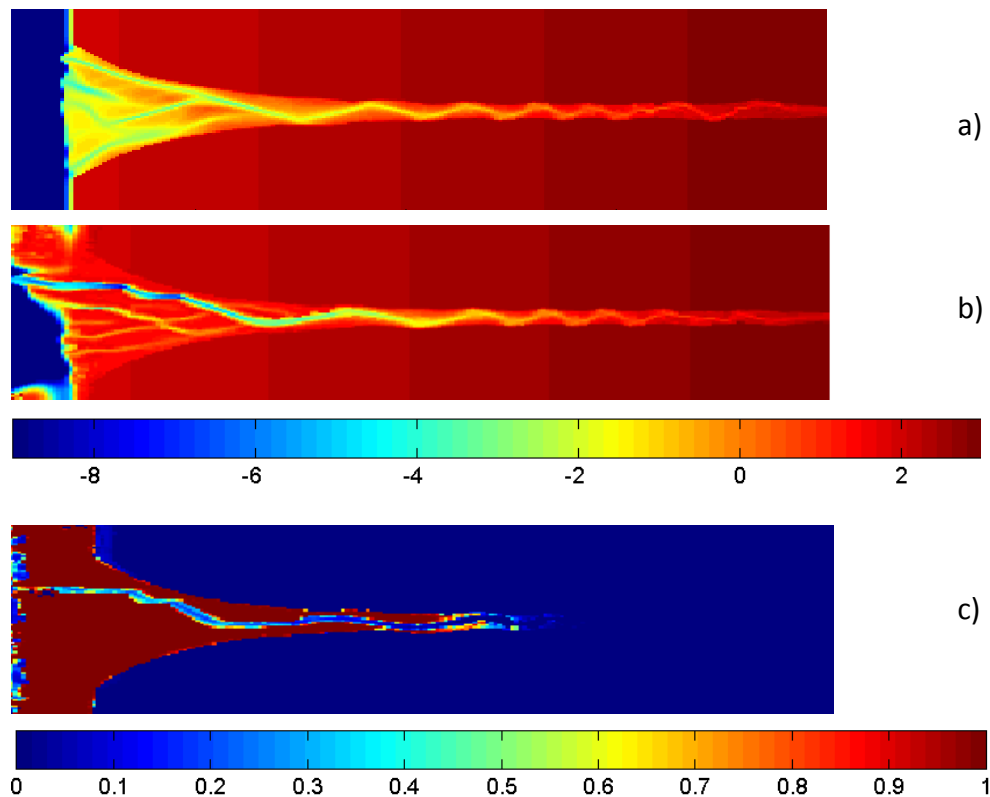
Figure 26: Rapid infilling of the estuary with cohesive sediment. a) bathymetry of simulation results with no mud influx, b) bathymetry of simulation results with mud influx, and c) deposits of mud in the estuary and seaward part.

Simulations with a relatively lower mud influx of 0.025 kg/m^3 from the western seaward boundary did not result in rapid estuary infilling after 2.9*10^5 tidal cycles (Figure 27 a). In this case the model was also driven by water level changes at the western boundary with a M2 tidal component and amplitude of 1.5 m. Although a lower sediment influx was used mud deposition took place at the northern seaward boundary (Figure 27 b). Therefore, alongshore tidal currents were also implemented in the next model run.

57
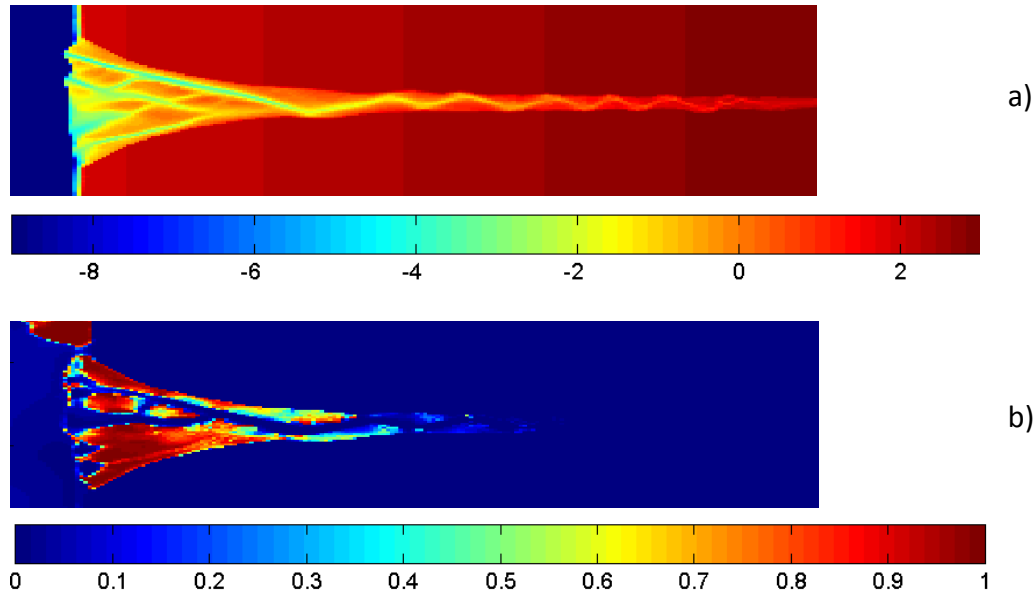
Figure 27: Mud deposition on northern boundary; a) bathymetry of the estuary, b) location of mud deposition.

Deposition of mud was prevented in the seaward part of the model by alongshore tidal wave propagation. Tidal currents flowing from either northern end to south end or in opposite direction during the turn of the tide was able to transport sediment through the boundaries and into the estuary. Two adjustments were needed to generate alongshore tidal wave propagation. These adjustments were: 1) increase the size of the seaward part, and 2) placing a phase difference for tides between the northern boundary and the southern boundary.

The dimensions of the seaward part was changed from 5 km by 3 km to a seaward dimension of 15km along the western end to 10 km along the northern and southern end. This increase was needed to prevent the boundaries from interfering with the currents within the seaward part (personal communication with Van der Vegt, M.). This seaward dimension had been kept the same during further morphodynamic simulations.

A phase difference was also needed between northern and southern seaward ends to generate a propagating tidal wave. This phase difference is determined by the following variables: tidal wavelength, the distance between the two seaward ends, and the waterdepth (Deltares, 2014). For this simulation the following variables were used: M2 tidal constituent, a distance of 15 km between the two seaward ends, and a waterdepth of 15 km. This resulted in a phase difference of 9.9 degrees.

The model resulted in an unrealistic erosion and shoal elevation in the seaward part when the phase difference was set to 9.9 degrees (see Figure 28). This unrealistic bathymetric development was simulated for $2.2*10^5$ tidal cycles and without mud influx. Two remedies

were used to prevent this unrealistic erosion in the seaward part; these remedies were: 1) decrease phase difference between the northern and southern seaward end, and 2) turn the western end into a closed boundary. The decrease in phase difference was needed to maintain a tidal range of 1.5 m. The closed boundary on the western end enabled the dominant directions of tidal currents to maintain a north-south direction for most of the time.
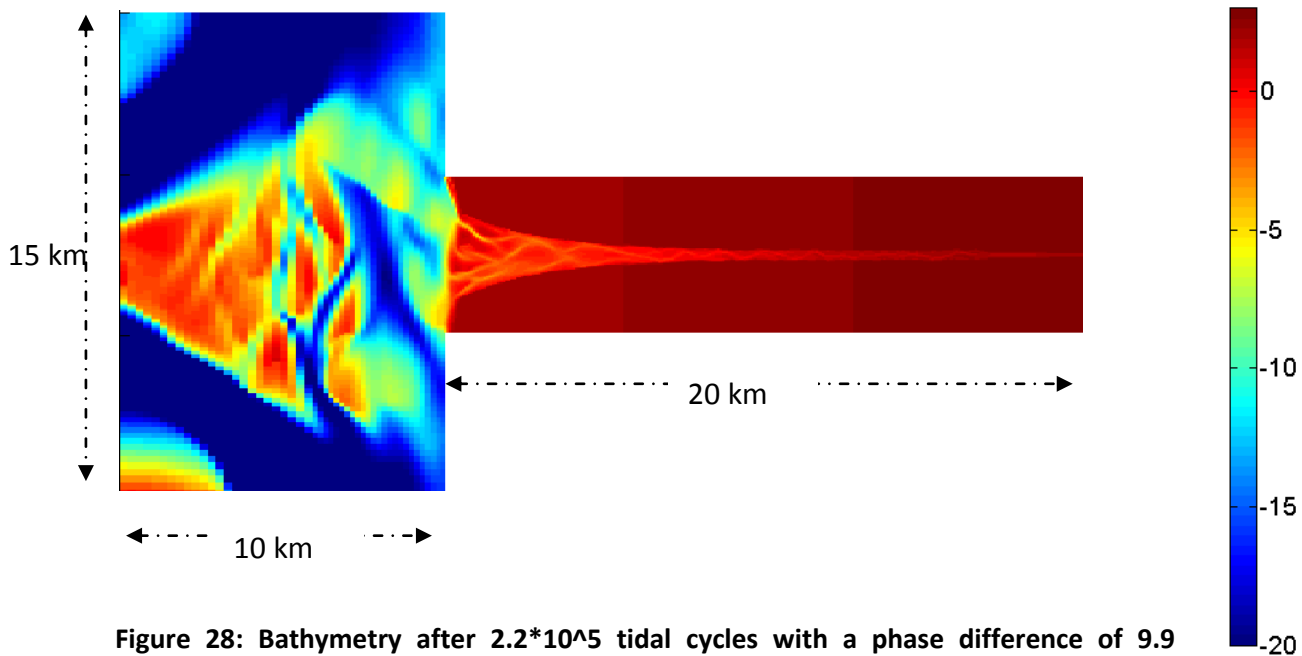
Figure 28: Bathymetry after 2.2*10^5 tidal cycles with a phase difference of 9.9 degrees.

The model results with the modified phase difference and western boundary did not show any unrealistic bed level changes in the seaward part (Figure 29). A harmonic tidal signal with a frequency of 30 deg/h was used to generate these morphological changes. Therefore, this configuration was used to simulate morphodynamic simulations with cohesive sediment influx and waves.

Waves were not simulated properly on the closed western boundary. The initial conditions for waves along the western end were set to a significant wave height of 4 m and a period of 6 seconds. However, the simulated wave heights were at the most 0.8 m and did not propagate into the estuary (see Figure 30). Therefore, the tidal flats in the model were not exposed to waves. The wave directions simulated by the model did propagate in the intended direction, which is towards the estuary. These settings were not further adjusted due to time constraints for this study.

Figure 29: Bathymetric changes after 2.9*10^5 tidal cycles. The model was run with a phase difference of 3 degrees, harmonic tide with frequency of 30 deg/h, and a closed western boundary.

Figure 30: Wave height and wave direction simulated by the Delft3d wave module
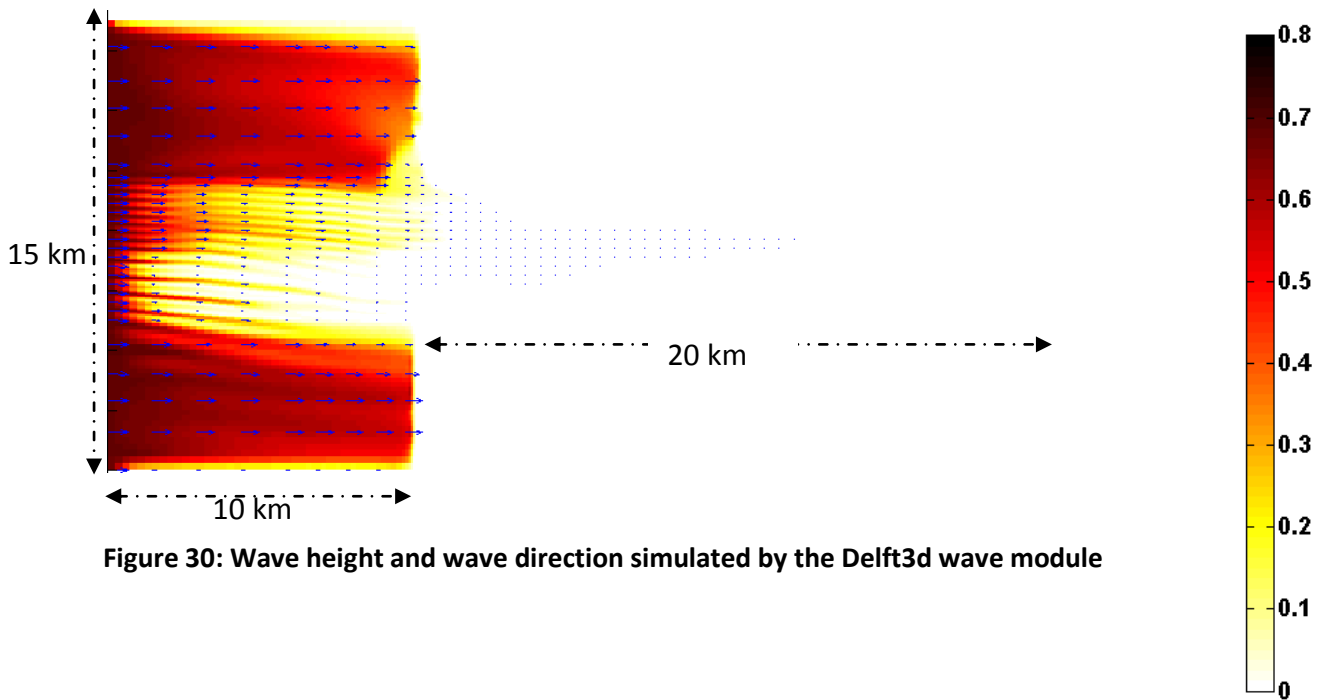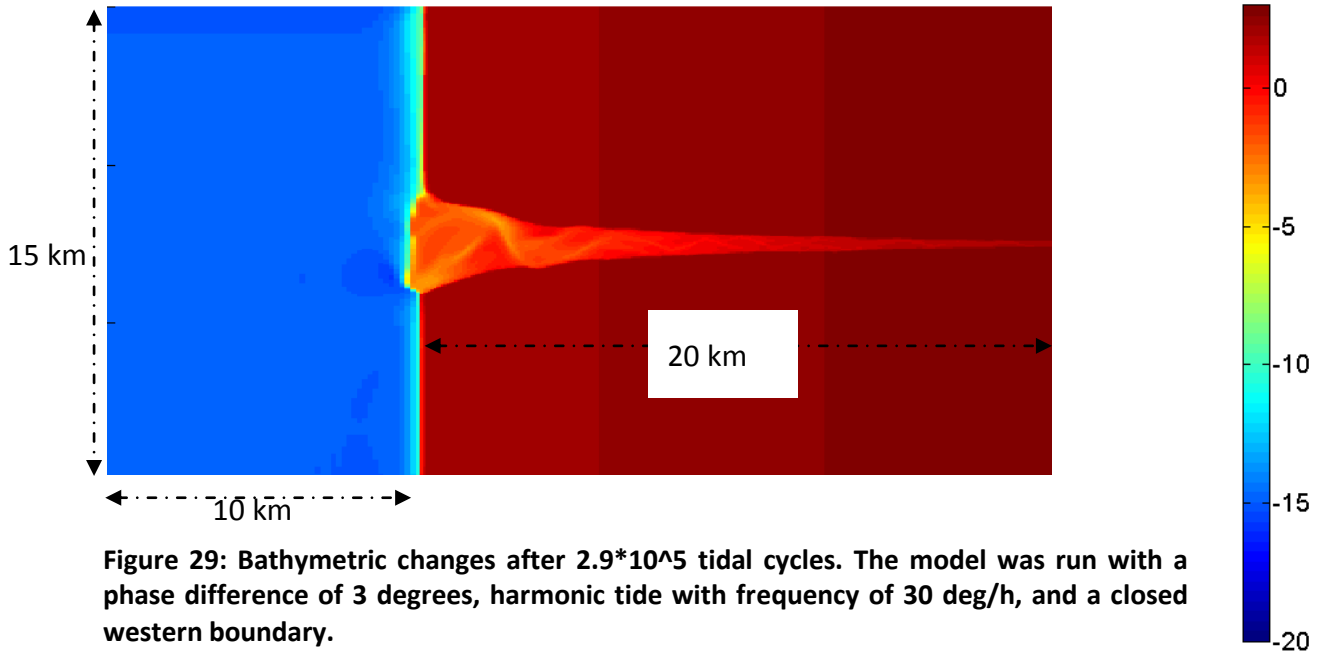
Discussion

Aim and Preliminary Conclusions from Results

The aim of this study was to analyze tidal flat width spatial differences in an estuary morphological composed of mixed non-cohesive and cohesive sediment. The simulated conditions were:

1) harmonic tidal fluctuations with only fluvial non-cohesive sediment influx
2) harmonic tidal fluctuations with both non-cohesive sediment and influx of marine cohesive sediment
3) combined harmonic fluctuations and offshore wave propagation with only fluvial non-cohesive sediment influx
4) combined harmonic fluctuations offshore landward wave propagation fluvial non-cohesive sediment influx and marine cohesive sediment influx.

This study did not take into account salinity differences in the estuary water which could influence suspended cohesive sediment transport. Furthermore the model did not explicitly take flocculation nor consolidation of cohesive sediment into account. The reader is referred to Delft3D-FLOW manual (Deltares 2014) for further details on the numerical model.

For the simulations with marine cohesive sediment influx the intertidal surface area increased compared to the simulations without marine cohesive sediment influx. The intertidal surface area was observed to have spatially different width and did not increase equally in alongshore estuary direction. See Figures 9 and 10 for an illustration of the models results for tide wave and cohesive sediment influx condition. For the simulations with cohesive sediment influx tidal mudflats were observed to be wider in the estuary mouth than further upstream. On the contrary, simulations with wave and cohesive sediment influx tidal mudflats are wider when going further upstream. Migrating channels also caused a local erosion of tidal mudflats. Therefore, a general equation for tidal mudflat width along an estuary needs to take migrating channels into account.

Alongshore suspended mud concentration was higher in the simulations with waves and mud influx than for the simulations with only mud influx. From these observations it could be noticed that under tidal conditions most of the marine cohesive sediment deposits in the seaward part in front of the estuary. Therefore, suspended cohesive sediment cannot be transported further inland by tidal currents. Water surface waves generated offshore are able to keep the deposited mud in suspension which enabled the tidal currents to carry the suspended mud suspension further upstream.

Channel and Tidal Mudflat Interaction

Previous studies have illustrated that tidal mudflat morphology under tidal and sediment influx can increase in height and width (Friedrichs & Aubrey 1995; Roberts et al. 2000; Pritchard & Hogg 2003; Bearman et al. 2010; Friedrichs 2011; Hu et. Al. 2015; Maan et al. 2015). In this study tidal mudflat have also been observed to increase in width and elevation when mud influx was present. However, in this study a numerical model simulated tidal mudflat formation from mud deposits in an estuary. The estuary channel bed in the model also consisted of sand on which shoals have developed. Shoal development in this study was similar to the study by Van der Wegen et al. (2008). These shoals deflect channel flow to shores or tidal mudflats which result in channel bank erosion. Erosion on one channel bank is balanced by deposition on another; lateral channel migration results from this sediment balance. Such lateral channel migration is comparable to the studies of meandering rivers by Van Dijk et al. (2013). These processes affect the length scales of width and depth of the estuary.

In this study the tidal mudflat width have been observed to mainly change from being wide and high elevated at the estuary mouth to narrow near the estuary head. This difference is attributed to the suspended cohesive sediment which is high near the estuary mouth and becomes lower near the estuary head. Maan et al. (2015) also illustrated tidal mudflat width to increase when mud influx was present. However, Maan et al. (2015) did not take alongshore tidal currents into account for tidal mudflat morphodynamics. In this study high bed shear stresses caused by a channel caused erosion of tidal mudflats. The elevation of tidal mudflat has not been reported in this research. This could have been done by making a graph with the hypsometry of the estuary. This hypsometry illustrates the area of estuary bed with elevation (Moore et al., 2008). The mud deposits have been observed to increase up to high water level which is similar to the studies by Mariotti & Fagherazzi (2013).

Van der Wegen et al. (2008) and Hibma et al. (2003) had illustrated that shoals form on sand channel beds. Shoals formation on the channel bed have also been observed in the model results of this study. These shoals deflect the flow towards channel banks thus increasing localized bed shear stresses. Different from studies by Townend (2010, 2012), Mariotti & Fagherazzi (2013), and Van der Wegen et al. (2014) these increased bed shear stresses erode channel bank and also mud deposits. On the other hand tidal mudflat accretion takes place on the locations where shoals are present. Figures 19 to 22 in this study illustrate channel bank erosion caused by lateral migrating channels. Simulations with cohesive sediment influx indicate that channel bank erosion is balanced by tidal flat accretion. How this tidal flat accretion scales with channel bend curvature has not been studied in this experiment.

The effect of cohesive sediment has been show by previous studies to increase channel bank erosion resistance and the overall change to morphology (Van Dijk et al. 2013; Caldwell & Edmons 2014). These studies have used morphological characteristics to indicate such effect. In similar way the simulations in this study has used the following parameters for tide dominated basins: length scale of channel width and depth and tidal prism (Hume 2005; Savenije 2012; Townend 2010 2012; Ridderinkhof et al. 2014). Higher length scales of the estuary width was found when cohesive sediment influx was absent compared to simulations with cohesive sediment influx. The tidal prisms follow the same trends for the length scales of width and depth; the tidal prism increases for simulations in which only sand influx is present and decreases when mud influx is added to the model (Figures 11). Several studies (Mariotti & Fagherazzi 2013; Lanzoni & D'Alpaos 2014) assume an initial tidal flat width or geometry for which is not clear how the initial geometries scale with overall estuary morphology.

Morphodynamic Equilibrium

Morphodynamic equilibrium is one approach to establish characteristic estuary morphology (Townend 2010 2012; Savenije 2012). However other morphological features can cause morphological changes with passing tidal cycles (Van der Wegen et al. 2008). Simulations in this study has also illustrated this continuous change in morphology. However energy dissipation theory has been adapted from Van der Wegen et al. (2008) to determine whether morphological changes still take place after a number of tidal cycles. This theory states that a minimum energy dissipation is needed to define morphodynamic equilibrium. In this study it has been illustrated that energy dissipation is sensitive to the length of estuary. Therefore it was not clear if tidal mudflats led the estuary morphodynamic to reach equilibrium. This indicates that a different morphodynamic equilibrium is needed for an estuary in which fluvial discharge is significant.

Conclusions

In this study the tidal mudflat width variation along the banks of an estuary have been studied. Marine mud influx, fluvial sand influx, tides and waves have been used to determine the morphological changes of the tidal mudflats within an estuary. The morphological changes to an estuary by the changes to the tidal mudflats have also been studied with the aid of length scales of width and depth, and tidal prism.

The marine mud suspended load is higher near the estuary mouth and smaller near the estuary head. The tidal mudflat widths follow these trends of suspended load. When the marine mud suspended load increases near the estuary head the tidal mudflat width had been observed to increase. However, when shoals form on the channel bed a concentrated tidal flow is directed towards the channel bank which results in an increased bed shear stresses on a channel bank. Erosion is induced on a small region on a channel bank and a tidal mudflat. Therefore, a localized narrowing of tidal mudflat takes place. The bed shear stresses on the shoals are lower to allow mud deposition which results in tidal mudflat accretion. Waves were not modeled to the proper significant wave height and did not propagate in the estuary. However, the modeled waves were significant to prevent mud from depositing in front of the estuary. Therefore, more mud was kept in suspension and transported further upstream. Mudflats did not form when mud influx was absent.

The length scale of width was higher when mud influx was absent and smaller when mud influx was present. However, the depth length scales were found to be smaller than the depth length scales for mud influx. The tidal prism shows a higher value for the simulations without mud than the simulations with mud influx. This indicated that estuary volume increased in time due to erosion.

Morphological changes in the simulations show a stable energy dissipation after $2*10^5$ tidal cycles. Whether tidal mudflats change the morphodynamic equilibrium of the simulated estuary is not clear with energy dissipation equation. First of all the results illustrated a morphodynamic equilibrium after $2*10^5$ tidal cycles and second changing the estuary length resulted in a lower energy dissipation. A possible cause of this contradiction is the inclusion of estuary which are less influenced by tidal currents. Clearer conditions for establishing a tidal limit is recommended.

References

Allen J.R.L. 2000. *Morphodynamics of Holocene Salt Marshes: A Review Sketch from the Atlantic and Southern North Sea Coasts of Europe Quaternary Science Reviews*. 19: 1155 - 1231

Bearman J. A. Friedrichs C.T. Jaffe B. E. Foxgrover A.C. 2010. *Spatial Trends in Tidal Flat Shape and Associated Environmental Parameters in South San Francisco Bay Journal of Coastal Research*. 26: 342-349.

Caldwell R.L. and D.A. Edmonds. 2014. *The Effects of Sediment Properties on Deltaic Processes and Morphologies: A Numerical Modeling Study*. J. Geophys. Res. Earth Surf. 119: 961–982. doi:10.1002/2013JF002965.

Cellino M. and W.H. Graf. 1999. *Sediment-Laden Flow in Open Channels Under Noncapacity and Capacity Conditions.* J. Hydr. Eng. 125:456-462.

Constantinescu G. Kashyap S. Tokyay T. Rennie C. D. Townsend R.D. 2013. *Hydrodynamic Processes and Sediment Erosion Mechanisms in an Open Channel Bend of Strong Curvature with Deformed Bathymetry*. Journal of Geophysical Research: Earth Surface. 118: 480–496. doi:10.1002/jgrf.20042.

Deltares. 2012. *Bed Module for Sand-Mud Mixtures In Framework Of Bwn Project NTW 1.3 Mud Dynamics.*

Deltares. 2014. Delft3D-FLOW user manual.

Deltares. 2014. Delft3D-WAVE Simulation of short-crested waves with SWAN user manual.

De Swart H.E. and J.T.F. Zimmerman. 2009. *Morphodynamics of Tidal Inlet Systems Annu. Rev. Fluid Mech*. 41:203–229. doi:10.1146/annurev.fluid.010908.165159

De Vriend H.J. 1996. *Mathematical Modelling of Meso-Tidal Barrier Island Coasts; Part 1: Emperical and Semi-Emperical Models*. In: Philip L. & Liu F. editors Advances in Coastal and Ocean Engineering. World Scientific Singapore p. 115- 150.

De Vriend H.J. and Ribberink J.S. 1996. *Mathematical Modelling Of Meso-Tidal Barrier Island Coasts; Part 2: Process-Based Simulation Models*. In: Philip L. & Liu F. editors Advances in Coastal and Ocean Engineering. World Scientific Singapore p. 151 – 193.

De Vriend H.J. 2001. *Long-Term Morphological Prediction*. In: Seminara G. & Blondeaux P. editors River Coastal and Estuarine Morphodynamics. Springer-Verlag Berlin Heidelberg p. 163 – 190.

Droppo I.G. 2001. *Rethinking What Constitutes Suspended Sediment Hydrological Processes*. 15: 1551– 564.

Edmonds D.A. and R.L. Slingerland. 2010. *Significant Effect of Sediment Cohesion on*

Delta Morphology. Nature Geoscience. 3: 105 – 109. DOI: 10.1038/NGEO730.

Friedrichs C. T. and D. G. Aubrey. 1995. *Uniform Bottom Shear Stress and Equilibrium Hyposometry of Intertidal Flat*s. In: Pattiaratchi Ch. editor Coastal and Estuarine Studies American Geophysical Union p. 405 – 429.

Friedrichs C.T. B.D. Armbrust H.E. de Swart. 1998. *Hydrodynamics and Equilibrium Sediment Dynamics of Shallow Funnel-Shaped Tidal Estuaries.* In: Dronkers and Scheffers editors Physics of Estuaries and Coastal Seas Balkema Rotterdam p. 315 – 327.

Friedrichs C.T. 2010. *Barotropic Tides in Channelized Estuaries*. In: Valle-Levinson editor Contemporary Issues in Estuarine Physics Cambridge University Press Cambridge p. 27 – 61.

Friedrichs C.T. 2011. *Tidal Flat Morphodynamics: A Synthesis*. In: E. Wolanski and D. McLusky editors Treatise on Estuarine and Coastal Science. Elsevier p. 138 – 170.

Grabowski R.C. I.G. Droppo G. Wharton. 2010. *Estimation of critical shear stress from cohesive strength meter-derived erosion thresholds.* Limnology and Oceanography-Methods. 8: 678–685.

Grabowski R.C.Droppo I.G. Wharton G. 2011. *Erodibility of cohesive sediment: The importance of sediment properties* Earth-Science Reviews. 105: 101–120. doi:10.1016/j.earscirev.2011.01.008.

Ha H.K. and J.P.-Y. Maa. 2009 *Evaluation of two conflicting paradigms for cohesive sediment deposition* Marine Geology. 265: 120 – 129. doi:10.1016/j.margeo.2009.07.001

Hibma A. Schuttelaars H.M. Wang Z.B. 2003. *Comparison of longitudinal equilibrium profiles of estuaries in idealized and process-based models* Ocean Dynamics. 53: 252–269. DOI 10.1007/s10236-003-0046-7

Hoyal D. C. J. D. and B. A. Sheets. 2009. *Morphodynamic evolution of experimental cohesive deltas* Journal of Geophysical Research. 114. doi:10.1029/2007JF000882.

Hu Z. Wang Z. B. Zitman T. J. Stive M. J. F. Bouma T.J. 2015. *Predicting long-term and short-term tidal flat morphodynamics using a dynamic equilibrium theory* Journal of Geophysical Research: Earth Surface. 120. doi:10.1002/2015JF003486

Kleinhans M.G. F. Schuurman W. Bakx H. Markies. 2009. *Meandering channel dynamics in highly cohesive sediment on an intertidal mud flat in the Westerschelde estuary* the Netherlands Geomorphology. 105: 261–276. doi:10.1016/j.geomorph.2008.10.005.

Kleinhans M.G. 2010. *Sorting out river channel patterns* Progress in Physical Geography. 34: 287–326. DOI: 10.1177/0309133310365300.

Kuijper C. R. Steijn D. Roelvink T. van der Kaaij P. Olijslagers. 2004. Morphological modelling of the Western Scheldt. Report. WL| delft hydraulics.

Lanzoni S. and A. D'Alpaos. 2014. *On funneling of tidal channels* J. Geophys. Res. Earth Surf. 120: 433–452. doi:10.1002/2014JF003203.

Lau Y.L. Droppo I.G. 2000. *Influence of antecedent conditions on critical shear stress of bed sediments* Water Research. 34: 663–667.

Maa J.P. Kwon J. Hwang K. Ha H. 2008. *Critical Bed-Shear Stress for Cohesive Sediment Deposition under Steady Flows* Journal of Hydraulic Engineering. 134: 1767 – 1771. DOI:10.1061/(ASCE)0733-9429(2008)134:12(1767)

Maan D.C. van Prooijen B.C. Wang Z.B.and De Vriend H. J. 2015. *Do intertidal flats ever reach equilibrium?* Journal of Geophysical Research: Earth Surface. 120: 2406–2436 doi:10.1002/2014JF003311.

Mariotti G. and S. Fagherazzi. 2012. *Channels-tidal flat sediment exchange: The channel spillover mechanism* JOURNAL OF GEOPHYSICAL RESEARCH. 117. doi:10.1029/2011JC007378.

Mariotti G. and S. Fagherazzi. 2013. *A two-point dynamic model for the coupled evolution of channels and tidal flats* JOURNAL OF GEOPHYSICAL RESEARCH: EARTH SURFACE. 118: 1387 – 1399. doi:10.1002/jgrf.20070.

Mehta A.J. Manning A.J. Yogesh P.K. 2014. *A note on the Krone deposition equation and significance of floc aggregation* Marine Geology. 354: 34 – 39. http://dx.doi.org/10.1016/j.margeo.2014.04.002

Mitchener H. and Torfs H. 1996. *Erosion of mud/sand mixtures* Coastal Engineering. 29: 1–25.

Nanson G.C. and Huang H.Q. 2008. *Least action principle equilibrium states iterative adjustment and the stability of alluvial channels* Earth Surf. Process. Landforms. 33: 923–942. doi: 10.1002/esp.1584.

Panagiotopoulos I. G. Voulgaris M.B. Collins. 1997. *The influence of clay on the threshold of movement of fine sandy beds* Coastal Engineering. 32: 19–43.

Pejrup M. and Mikkelsen O.A. 2010. *Factors controlling the field settling velocity of cohesive sediment in estuaries Estuarine Coastal and Shelf Science*. 87: 177–185. doi:10.1016/j.ecss.2009.09.028.

Pittaluga M. B. Tambroni N. Canestrelli A. Slingerland R. Lanzoni S. Seminara G. 2015. *Where river and tide meet: The morphodynamic equilibrium of alluvial estuaries.* Journal of Geophysical Research: Earth Surface. 120: 75–94. doi:10.1002/2014JF003233.

Postma H. 1961. *Transport and Accumulation of Suspended Matter in the Dutch Wadden Sea*. Netherlands Journal of Sea Research. 1: 148 – 190.

Pritchard D. A.J. Hogg W. Roberts. 2002. *Morphological modelling of intertidal mudflats: the role of cross-shore tidal currents* Continental Shelf Research. 22: 1887–1895.

Pritchard D. and A. J. Hogg. 2003. *Cross-shore sediment transport and the equilibrium morphology of mudflats under tidal currents* JOURNAL OF GEOPHYSICAL RESEARCH. 108. doi:10.1029/2002JC001570.

Ridderinkhof W. H. E. de Swart M. van der Vegt N. C. Alebregtse P. Hoekstra. 2014. *Geometry of tidal inlet systems: A key factor for the net sediment transport in tidal inlets* J. Geophys. Res. Oceans. 119: 6988–7006. doi:10.1002/2014JC010226.

Roberts W. Le Hir P. Whitehouse R.J.S. 2000. *Investigation using simple mathematical models of the effect of tidal currents and waves on the profile shape of intertidal mudflats Continental Shelf Research.* 20: 1079-1097

Savenije H.H.G. 2012. *SALINITY AND TIDES IN ALLUVIAL ESTUARIES* Delft University of Technology Water Resources Section Delft The Netherlands.

Seminara G. S. Lanzoni M. Bolla Pittaluga L. Solari. 2001. *Estuarine Patterns: An Introduction to their Morphology and Mechanics*. In: Balmforth N. J. and A. Provenzale editors Geomorphological Fluid Mechanics. Springers. p. 455-499. Doi: 10.1007/3-540-45670-8

Stover Christopher and Weisstein Eric W. "*Cartesian Coordinates*." From MathWorld--A Wolfram Web Resource. http://mathworld.wolfram.com/CartesianCoordinates.html

Toorman E.A. 2000. *SOME THOUGHTS ON THE MODELLING OF EROSION AND DEPOSITION OF COHESIVE SEDIMENTS*. Report. Hydraulics Laboratory Civil Engineering Department Katholieke Universiteit Leuven.

Torfs H. 1995. *Erosion of Mud/Sand Mixtures*. Ph.D. thesis Katholieke Universiteit Leuven faculteit der Toegepaste Wetenschappen Departement Burgelijke Bouwkunde Laboratorium voor Hydraulica.

Townend I. 2010. *An Exploration of Equilibrium in Venice Lagoon Using an Idealised Form Model Continental Shelf Research*. 30. 984 – 999.

Townend I. 2012. *The Estimation of Estuary Dimensions Using a Simplified Form Model and the Exogenous Controls Earth Surf*. Process. Landforms. 37: 1573–1583. DOI: 10.1002/esp.3256.

Tambroni N. and G. Seminara. 2012. *A One-Dimensional Eco-Geomorphic Model of Marsh Response to Sea Level Rise: Wind Effects Dynamics of the Marsh Border and Equilibrium* JOURNAL OF GEOPHYSICAL RESEARCH. 117. doi:10.1029/2012JF002363.

van der Wegen M. and B. E. Jaffe. 2014. *Processes Governing Decadal-Scale Depositional Narrowing of the Major Tidal Channel in San Pablo Bay California USA* J. Geophys. Res. Earth Surf. 119: 1136–1154. doi:10.1002/2013JF002824.

van Dijk W.M I.W. van de Lageweg and M.G. Kleinhans. 2013. *Formation of a Cohesive Floodplain in a Dynamic Experimental Meandering River Earth Surf*. Process. Landforms 38: 1550–1565. Doi:10.1002/esp.3400.

van Kessel Th. Van lede J. de Kok J. 2011. *Development of a Mud Transport Model for the Scheldt Estuary Continental Shelf Research*. 31: S165–S181. doi:10.1016/j.csr.2010.12.006

Van Ledden M. 2002. *A Process-Based Sand-Mud Model*. In: J.C. Winterwerp and C. Kranenburg editors Fine Sediment Dynamics in the Marine Environment p. 577 – 594.

Wang Z.B. Van Maren D.S.Ding P.X. Yang S.L.Van Prooijen B.C. De Vet P.L.M. Winterwerp J.C. De Vriend H.J. Stive M.J.F. Hec Q. 2015. *Human Impacts on Morphodynamic Thresholds in Estuarine Systems Continental Shelf Research*. 111: 174–183. doi:10.1016/j.csr.2015.08.009.

Winterwerp J.C. and van Kesteren W.G.M. 2004. *Introduction to the Physics of Cohesive Sediment in the Marine Environment*. WL / Delft Hydraulics & Delft University of Technology. Delft THE Netherlands.

Winterwerp J.C. 2007. *On The Sedimentation Rate of Cohesive Sediment*. In: Maa J.P.-Y. L.P. Sanford and D.H. Schoellhamer editors Estuarine and Coastal Fine Sediments Dynamics Elsevier p. 209 – 226.

Appendix 1 Model Parameter Settings for Morphology

Table of main parameters and values			
	Value	Unit	Comments
Hydrodynamic parameters			
Gravity	9.81	m/s^2	
Water density	1000	Kg/m^3	
Beta_c	0.5	No unit	
Bottom roughness			
Chezy (U-direction)	50		Uniform
Chezy (V-direction)	50		Uniform
Wall roughness			
Slip condition	Free		
Background horizontal viscosity/diffusivity			
Horizontal eddy viscosity	1	_m2/s	Uniform
Horizontal eddy diffusivity	10	_m2/s	Uniform
Sediment parameters			
Sediment 1			Non-cohesive sediment
Reference density for hindered settling	1600	Kg/m^3	
Specific density	2650	Kg/m^3	
Dry bed density	1600	Kg/m^3	
Median sediment diameter	300	_μm	D50

Sediment 2			Cohesive sediment
Reference density for hindered settling	1600	Kg/m^3	
Specific density	2650	Kg/m^3	
Dry bed density	1600	Kg/m^3	
Fresh settling velocity	0.25	_mm/s	
Critical bed shear stress for sedimentation	1000	N/m2	Uniform
Critical bed shear stress for erosion	0.2	N/m2	Uniform
Erosion parameter	0.0001	$Kg/m^{-2}s^{-1}$	Uniform
Initial sediment layer thickness at bed	0.05	_m	Uniform
Morphology			
Update bathymetry during FLOW simulation			Checked
Equilibrium sand concentration profile at inflow boundaries			Checked
Morphological scale factor (MORFAC)	400	No unit	
Spin-up time before morphological changes	14400	Min	
Minimum depth for sediment calculation (SedThr)	0.05	M	
Sediment transport parameters			

Van Rijn's reference height factor	1	No unit	
Threshold sediment thickness	0.05	M	
Estimated ripple height factor	2	No unit	
Sediment transport formulas			
Engelund-Hansen (1967)			
Calibration coefficient	1	No unit	
bed roughness height (dummy)	0.05	m	
Multiplication (calibration) factors			
Factor for erosion of adjacent dry cells	0.5	No unit	
Current-related reference concentration factor	1	No unit	
Current-related transport vector magnitude factor	1	No unit	
Wave-related suspended transport factor	1	No unit	
Wave-related bed-load transport factor	1	No unit	